HHS Public Access

Thiol-Michael Addition Microparticles: Their Synthesis, Characterization, and Uptake by Macrophages

Emerson L. Grey[a], **Jazalle McClendon**[b], **Joshita Suresh**[a], **Scott Alper**[c], **William J. Janssen**[b,d], **Stephanie J. Bryant**[a,e,f,*]

[a]Department of Chemical and Biological Engineering, University of Colorado, 3415 Colorado Ave, Boulder, CO 80309-0596, USA

[b]Division of Pulmonary, Critical Care, and Sleep Medicine, Department of Medicine, National Jewish Health, 1400 Jackson St, Denver, CO 80206, USA

[c]Department of Immunology and Genomic Medicine, Center for Genes, Environment and Health, National Jewish Health, 1400 Jackson St, Denver, CO 80206, USA

[d]Department of Medicine, University of Colorado Anschutz Medical Campus, 12631 East 17th Avenue, Aurora, CO 80045, USA

[e]Materials Science & Engineering Program, University of Colorado, 4001 Discovery Dr, Boulder, CO 80309-0613, USA

[f]BioFrontiers Institute, University of Colorado, 3415 Colorado Ave, Boulder, CO 80309-0596, USA

Abstract

Polymeric microparticles are promising biomaterial platforms for targeting macrophages in the treatment of disease. This study investigates microparticles formed by a thiol-Michael addition step-growth polymerization reaction with tunable physiochemical properties and their uptake by macrophages. The hexafunctional thiol monomer dipentaerythritol hexa-3-mercaptopropionate (DPHMP) and tetrafunctional acrylate monomer di(trimethylolpropane) tetraacrylate (DTPTA) were reacted in a stepwise dispersion polymerization, achieving tunable monodisperse particles over a size range (1–10 μm) relevant for targeting macrophages. An off-stoichiometry thiol-acrylate reaction afforded facile secondary chemical functionalization to create particles with different chemical moieties. Uptake of the microparticles by RAW 264.7 macrophages was highly dependent on treatment time, particle size, and particle chemistry with amide, carboxyl, and thiol terminal chemistries. The amide-terminated particles were non-inflammatory, while the carboxyl and thiol-terminated particles induced pro-inflammatory cytokine production in conjunction with particle phagocytosis. Finally, a lung-specific application was explored through time-dependent uptake of amide-terminated particles by human alveolar macrophages *in vitro* and mouse lungs *in vivo* without inducing inflammation. The findings demonstrate a promising microparticulate

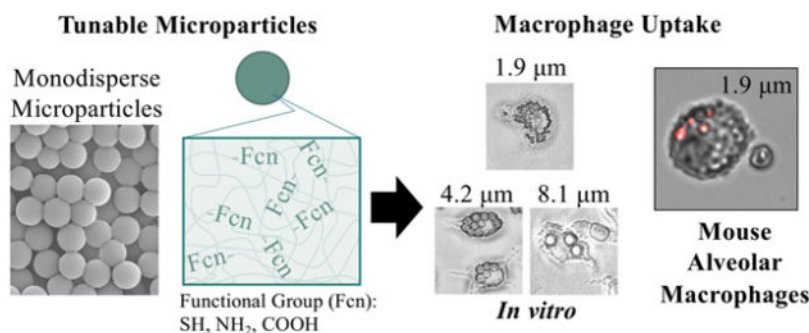*Corresponding Author*: stephanie.bryant@colorado.edu.

delivery vehicle that is cyto-compatible, non-inflammatory, and exhibits high rates of uptake by macrophages.

Graphical Abstract

Keywords

microparticles; thiol-Michael addition; phagocytosis; RAW 264.7 macrophages; human alveolar macrophage; lung

1. INTRODUCTION

Polymeric microparticles can serve as vehicles by which to transport therapeutics targeting macrophages in disease. Microparticles, which are typically defined by a diameter 0.5 μm, provide increased payload capacity relative to free drug while protecting the encapsulated therapeutic from rapid degradation.[1,2] Due to their size range being similar to that of pathogens,[3] microparticles can also provide non-specific, yet targeted uptake to phagocytic cells. In disease, macrophages are key players for modulating immune responses associated with inflammation, cancer, and infection.[3–6] In their role as scavengers, the primary mechanism by which macrophages uptake microparticles is through phagocytosis.[7] Phagocytosis involves a two-step process with particle attachment to the plasma membrane followed by their engulfment through an actin-myosin driven process.[8] A number of studies have shown that targeting macrophages with drug-loaded microparticles can be beneficial. For example, phagocytosis can result in much higher drug concentrations within macrophages compared to free drug.[9] Anti-inflammatory drug-loaded microparticles have been successful at altering the polarization state of macrophages from pro-inflammatory to anti-inflammatory.[10] Importantly, studies have shown that monocytes/macrophages can retain microparticles long-term and that drugs once released from the particles can escape the phagosome and even be released extracellularly over multiple weeks.[11] Taken together, microparticles offer an exciting therapeutic approach to target macrophages.

The physiochemical properties of microparticles (e.g., size, chemistry, shape, and stiffness) influence the extent of particle phagocytosis by macrophages. Generally, microparticles in the range of 1–5 μm are rapidly phagocytosed by macrophages while those that are smaller or larger require longer times.[4,12,13] Within this range, diameters around 2 μm often have the greatest uptake; this is attributed to the ability of these particles to attach between the ruffles

on the cell membrane, increasing the surface area of attachment.[12] Large particles (>10 μm) are generally not readily phagocytosed and instead remain attached to the cell membrane, which can induce an inflammatory response in macrophages that is not observed by smaller phagocytosed particles.[14] To study the role of chemistry on phagocytosis, functionalized polystyrene nano and microparticles are commonly used. A positive correlation with zeta potential from different functionalized polystyrene nanoparticle and uptake by human THP-1 derived macrophages was reported, indicating that particle surface charge plays a key role in phagocytosis.[15] When similar nanoparticles were delivered to the lungs of rats, a positive correlation was again found between zeta potential and neutrophil numbers as well as pro-inflammatory cytokine levels within the bronchoalveolar lavage (BAL) fluid; this suggests that as particle charge becomes more positive, a stronger inflammatory response is induced.[16] Makino *et al.*[17] measured superoxide anion production as an indicator of phagocytosis and found higher production levels in rat alveolar macrophages exposed to charged (amine or carboxyl) polystyrene microparticles compared to neutral and unmodified particles. Together, charged particles (negative or positive) induce higher phagocytic activity, while positively charged particles appear to be more inflammatory.

Poly(lactic-co-glycolic acid) (PLGA) microparticles are among the most common microparticles used clinically for drug delivery.[18,19] Similar to polystyrene microparticles, PLGA microparticles have shown a strong dependence of particle size and surface modification on phagocytosis. For example, Hirota *et al.*[20] demonstrated that NR8383 alveolar macrophages phagocytosed PLGA microparticles with a mean diameter of 1 and 3 μm to a greater extent than 6 μm microparticles and even more so than 10 μm microparticles. Sun *et al.*[21] found that 0.5 μm PLGA particles were more readily taken up by RAW 264.7 macrophages than those with a 2 μm diameter. When the surface charge of PLGA microparticles was modified from neutral to cationic with poly-L-lysine, the positively charged microparticles were more easily internalized by THP-1 macrophages than those with the unmodified formulation.[22] Despite their wide use clinically, shortcomings of PGLA microparticles include their low yields and broad polydispersity. Although methods for synthesizing PLGA microparticles using emulsification have improved size uniformity,[23,24] the particles are still polydisperse such that studies have reported polydispersity indices of 0.17–0.21.[23]

While macrophages readily phagocytose different types of microparticles, their physiochemical properties, notably size and chemistry, can be used to tune the timing and the extent of phagocytosis for a desired application. It is important to note that other physical properties of microparticles have been shown to influence phagocytosis. Notably, spherical particles are more readily phagocytosed than non-spherical particles with high aspect ratios[25–27] and rigid microparticles are more readily taken up by macrophages when compared to soft deformable particles.[28] However, size and chemistry appear to be the dominating physicochemical properties that determine the rate and extent of particle uptake. Thus, polymeric microparticle formulations that afford tight control over their properties could improve upon existing therapeutic microparticles (e.g., PLGA). One potential alternative is the use of click reactions to form microparticles. These reactions afford orthogonality and specificity, have minimal if any side products, and exhibit high yields under mild reaction conditions.[29,30] The versatility of click chemistries to enable

microparticle fabrication and surface modification has been documented.[31–37] For example, Wang *et al.*[38,39] utilized the thiol-Michael-addition click reaction combined with dispersion polymerization as a facile approach to fabricate microparticles with low polydispersity. The size of the microparticles was readily tuned by varying the monomer concentration during synthesis, and adjusting the stoichiometric ratio of the monomers allowed for different network-terminating functionalities (i.e., thiols or acrylates). The feasibility of these thiol-Michael addition microparticles as a DNA delivery vehicle to macrophages was recently demonstrated.[40] Therefore, this highly customizable microparticle platform is one promising approach for targeting macrophages, but has yet to be explored.

This study examines the physiochemical properties of microparticles formed by thiol-Michael addition step-growth polymerization reaction prepared by reacting low molecular weight multi-functional thiol and acrylate monomers, which produce highly crosslinked rigid particles, using dispersion polymerization to form spherical particles.[38,39] By reacting the monomers at different concentrations and stoichiometries, microparticles of various sizes and chemical functionalities were produced, resulting in free thiol, amide, and carboxylic acid terminated groups. The particles were characterized by their size, polydispersity, chemistry, zeta potential, and stability at pH relevant to the phagosome (i.e., acidic). *In vitro* studies were performed with RAW 264.7 murine macrophages to evaluate the effects of particle size and chemistry on macrophage metabolic activity (as an indicator of cell viability/proliferation), inflammatory response, and phagocytosis. Macrophages were also stimulated with lipopolysaccharide (LPS) which was used to simulate the inflammatory environment *in vivo*. To test the relevance of these microparticles for lung-specific applications, amide functionalized microparticles were exposed to human alveolar macrophages *in vitro* and mice intratracheally with and without LPS stimulation. Inflammatory responses and particle uptake were assessed. Overall, this study demonstrates that this highly tunable polymeric microparticle system, which produces monodisperse and cytocompatible microparticles, is readily taken up by macrophages and, depending on the terminated group chemistry, without eliciting an inflammatory response. These microparticles were also taken up to a greater extent by inflammatory macrophages. In summary, these highly tunable microparticles are a promising platform for targeting macrophages, including those that are inflammatory and those residing in the lungs.

2. EXPERIMENTAL SECTION

2.1. Materials.

Di(trimethylolpropane) tetraacrylate (DTPTA), triethylamine (TEA), polyvinylpyrrolidone (PVP), 4-methoxyphenol (MeHQ), iodoacetamide, potassium dihydrogen phosphate, sodium citrate, sodium acetate, and dansylcadaverine were purchased from Sigma Aldrich. Fluoraldehyde™ o-Phthaldialdehyde Reagent Solution (OPA); alamarBlue™ Cell Viability Reagent; 2-iminothiolane (Pierce™ Traut's Reagent); 5,5'-Dithiobis-(2-Nitrobenzoic Acid) (DTNB; Ellman's Reagent); methanol; potassium phosphate, dibasic; citric acid; acetic acid; and ethylenediaminetetraacetic acid (EDTA) were purchased from Fisher Scientific. Tetramethylrhodamine-5-(and −6) C2 maleimide was purchased from Anaspec Inc. 3-mercaptopropionic acid was purchased from Alfa Aesar. Dipentaerythritol hexa-3-

mercaptopropionate (DPHMP) was procured from Tokyo Chemical Industry. Dulbecco's phosphate buffered saline (DPBS), Dulbecco's Modified Eagle's Medium (DMEM), glutagro, and penicillin/streptomycin were purchased from Corning. Dimethyl sulfoxide (DMSO) was purchased from VWR International. RAW 264.7 macrophages were obtained from ATCC. Fetal bovine serum (FBS) was procured from Atlanta Biologics. Mouse IL-6 and TNF-α and human IL-6 and TNF-α Duo Set ELISA kits were purchased from R&D Systems. LPS from *E. coli* O111:B4 (LPS-EB) was obtained from InvivoGen for *in vitro* studies and LPS from *E. coli* O55:B5 was purchased from List Biological Laboratories for *in vivo* studies. Isoflurane was from Baxter. Jenner Stain Working Solution, Giemsa Stain Stock Solution, and Acetic Acid 1% Aqueous were procured from Poly Scientific R&D Corp. CD45 FITC, CD64 BV711, CD88 BUV 395, SiglecF BV421, CD11b APC, and Ly6G PECy7 monoclonal antibodies were obtained from BD Biosciences.

2.2. Microparticle synthesis.

DTPTA, PVP (a surfactant), and MeHQ (a radical inhibitor) were combined and dissolved in methanol in a round bottom flask. DPHMP was dissolved in methanol to improve solubility and then transferred to the reaction mixture. TEA (a catalyst) was next added to the reaction mixture. The final concentration in the reaction mixture was 0.4 – 15 g/g (wt %) monomer (DPHMP and DTPTA), 15 wt% PVP, 5 wt% TEA, and 5 wt% MeHQ. The moles of the sulfhydryl to the moles of acrylate were varied by 1.2:1, 1.33:1, 1:1.2, or 1:1.33 (sulfhydryl functional group : acrylate functional group) to create particles with 20% or 33% excess sulfhydryl or acrylate terminal groups. Each particle formulation was used for different studies, which is denoted in the following sections. The reaction progressed for a minimum of five hours with continuous magnetic stirring in ambient conditions. Particles were recovered by centrifugation and then rinsed 3x in fresh methanol by vortexing or sonicating followed by centrifugation after each rinse step.

2.3. Amide-functionalized particles.

Sulfhydryl-terminated (33% excess thiols) microparticles were transferred from methanol to DMSO using progressively higher ratios of DMSO to methanol until the particles were fully suspended at 21 mg particle/mL of DMSO. Each step involved vortexing and centrifugation. In a round bottom flask protected from light, iodoacetamide was dissolved in DMSO at 44 mg/mL by magnetic stirring, then an equal volume of particles in DMSO was added. Additional DMSO was used to rinse the vessel containing the particles. The final particle concentration in the reaction was 8.5 mg particle/mL in 50 ml DMSO. The reaction was allowed to progress until the solution transitioned from a clear to amber color, approximately 48 hours, and terminated by washing the particles via centrifugation in DMSO.

2.4. Carboxyl-functionalized particles.

Acrylate-terminated (33% excess acrylates) microparticles were reacted (8 mg particle/mL) with 1% g/v 3-mercaptopropionic acid in the presence of the catalyst TEA at 5 wt% in methanol (50 mL reaction volume) for 24 hours. The resultant particles were used for zeta potential and swelling studies. To increase the extent of the reaction for the *in vitro* studies, particles were synthesized with 2% g/v 3-mercaptopropionic acid and 5 wt% TEA and

reacted for 72 hours. The particles were recovered by rinsing via centrifugation with filtered methanol to remove excess reactant.

2.5. Fourier transform infrared spectroscopy (FTIR).

Fourier Transform Infrared (FTIR) spectroscopy was performed using a Nicolet iS20 to confirm the functionalization of the particles. In brief, particles were applied dropwise to salt plates in a uniform layer and dried under nitrogen, then FTIR spectra were collected. The presence or absence of sulfhydryl peak (2550–2600 cm^{-1})[39] was used to confirm that sulfhydryl groups had been consumed during amide functionalization of excess sulfhydryl particles. The acrylate peak at 810 cm^{-1} was used to confirm that acrylate groups[39] were consumed following carboxyl functionalization of excess acrylate particles. To monitor reaction of acrylate to carboxyl, FTIR with attenuated total reflection (ATR) was used. In brief, aliquots of microparticles were taken at time intervals for 72 hours, immediately rinsed via centrifugation 3x with methanol, and then dried into pellets under ambient conditions. The sulfhydryl (2550–2600 cm^{-1}) and acrylate (810 cm^{-1}) peaks were monitored over time and compared with those corresponding to the unreacted particles.

2.6. Fluorescent microparticle synthesis.

Microparticles with 33% excess sulfhydryl were suspended in DMSO and reacted with tetramethylrhodamine-5-(and −6) C2 maleimide at a 500:1 molar ratio (sulfhydryl:maleimide). The reaction mixture was protected from light and stirred for 24 hours. The particles were rinsed several times via centrifugation with DMSO to remove unreacted fluorophore. The same protocol was followed for amide-functionalized particles by reacting the residual thiols with maleimide. Carboxyl-functionalized particles were labeled with dansylcadaverine. In brief, 14.2 mg Traut's reagent (1.5 mg/mL) were dissolved in DPBS (9.75 mL) containing 2.5 mM EDTA, pH 8.0, with stirring in a round bottom flask protected from light. Dansylcadaverine (35 mg/mL) was dissolved in anhydrous DMSO (0.25 mL), then added dropwise to the reaction mixture. After 1 hour, carboxyl-functionalized particles (16 mg particles/mL) suspended in the same DPBS buffer (14 mL) were added to the reaction mixture and reacted for 5 hours. The particles were rinsed via centrifugation several times with fresh buffer to remove unreacted fluorophore.

2.7. Microparticle size by scanning electron microscopy (SEM).

Microparticles in methanol were applied dropwise to a silicon wafer and dried under nitrogen. The particles were sputter coated with 1–2 nm platinum and then imaged with a Hitachi SU3500 Scanning Electon Microscope. For each experimental group, diameters (n=300–3750) were measured in ImageJ and fit to normal distributions in MATLAB. Poly dispersity index (PDI) was calculated as $(\sigma/\overline{x})^2$, where σ is the standard deviation and $\overline{x}$ is the average particle diameter.

2.8. Microparticle degradation.

Microparticles with 20% excess acrylate or sulfhydryl groups were rinsed via centrifugation to 0.1 M acetate buffer (pH 4 and 5), 0.1 M citrate buffer (pH 6), or DPBS (pH 7). Particles were equilibrated to the buffers by rinsing 3x at the initiation of the study. Every two

days for fourteen days, particle aliquots were removed, rinsed via centrifugation in buffer 3x, then deionized filtered water 3x, and finally in methanol 3x. The particles were dried by evaporation onto silicon wafer, sputter coated with platinum, and imaged with SEM. Diameters (n=300 particles per formulation) were measured with ImageJ.

2.9. Zeta potential.

Microparticles were dispersed in pH-adjusted buffers at 4 mg/mL and then analyzed on an Anton Paar Litesizer 500 at 21.7 °C (sample = 1 aliquot of microparticles per pH). The samples were run in automatic mode with Smoluchowski approximation a maximum of 1000 times per sample. Buffers at pH 3, 4, 5, and 6 were prepared with 0.1 M citrate-sodium citrate and adjusted with 1 M HCl and/or 1 M NaOH as necessary. Buffers at pH 7, 8, and 9 were prepared with 0.1 M Tris-HCl and adjusted with 1 M NaOH and/or 1 M HCl as necessary. Zeta potential was also measured in de-ionized water (sample size = 4) under the same parameters.

2.10. Sulfhydryl quantification.

Microparticles dispersed in filtered DI water were assayed using Ellman's assay following the manufacturer's protocol. A volume of 500 μL of microparticles with concentration 1–16 mg/mL in filtered DI water was reacted with Ellman's reagent at room temperature for two hours. After the reaction, the particles were centrifuged, and the supernatant was collected. A volume of 200 μL of supernatant was assayed by measuring absorbance at 412 nm and compared to a standard curve to determine sulfhydryl concentration.

2.11. Mass swelling.

Microparticles in methanol were rinsed via centrifugation to filtered DI water and allowed to equilibrate for 24 hours. Aliquots of microparticles were centrifuged, supernatant discarded, and swollen masses measured. The particles were then lyophilized and their dry masses were measured. The mass swelling ratio was calculated by mass of swollen particles divided by mass of dry particles.

2.12. Preparation of particles for cellular uptake.

Fluorescent microparticles in methanol or DMSO were transferred to filtered DI water by centrifugation. The particles were then transferred to 70% ethanol by centrifugation and soaked therein overnight for sterilization. Sterile microparticles were then transferred via centrifugation to sterile filtered DI water and then to sterile DPBS, and then soaked in sterile DPBS overnight. Finally, particles were rinsed via centrifugation 3x with sterile DPBS. Known volume aliquots of the resultant particle stock were lyophilized to determine microparticle concentration.

2.13. In vitro microparticle treatment of RAW 264.7 macrophages.

RAW 264.7 murine macrophages were cultured in DMEM with 10% FBS and 1% penicillin/ streptomycin at 37 °C and 5% CO_2. Cells were seeded in 6 or 96-well plates at 47,000 cells/cm^2 and allowed to adhere overnight. After 24 hours, medium was changed to DMEM medium with 10% FBS and 1% antibiotic-antimycotic. Cells were cultured for

two additional days prior to treatment. At the time of treatment, the medium was refreshed. The cells were treated with or without 1 μg/mL LPS in the same medium for 30 minutes and then with or without 55 μg/mL microparticles in PBS for 6 or 24 hours. Media were collected and flash frozen for ELISAs and cells were either disassociated from the TCPS with Accumax, scraped, and fixed with 4% PFA for flow cytometry or fixed directly in the plate for staining and imaging.

2.14. Human alveolar macrophages and in vitro treatment with microparticles.

Alveolar macrophages were obtained from the National Jewish Human Lung Tissue Consortium and were isolated from deceased organ donors as previously described in detail.[41] Lungs were selected from non-smoking organ donors that had no history of pulmonary disease and that died in the hospital from non-pulmonary causes. Lungs were removed at the time of death and processed within 24 hours. To obtain alveolar macrophages, PBS was instilled into lung lobes via a central bronchus and lavage fluid was collected in sterile containers. Lavage fluid was sequentially filtered through sterile gauze and a 70-micron sterile filter to eliminate mucus. Fluid was centrifuged to pellet cells at 300xg for 5 min. Cells were resuspended in PBS, quantified, and then washed a second time in PBS. Cell pellets were resuspended at a concentration of 53×10^6 cells/mL in freezing medium (50% DMEM, 40% FBS, 10% DMSO) and then preserved at −140 °C until use. Human alveolar macrophages were seeded from frozen in DMEM medium with 5% FBS and 1% antibiotic-antimycotic at 210,000 cells/cm^2 in 6 and 96-well TCPS plates. Human alveolar macrophages were treated with and without LPS and with and without microparticles as described above for the RAW 264.7 cells.

2.15. Macrophage metabolic activity.

Following microparticle treatment, cells in 96-well plates were rinsed with DPBS and 10% alamarBlue reagent in DMEM medium was applied. After 6 hours, absorbance was read at 570 and 600 nm and metabolic activity was calculated per manufacturer instructions. Metabolic activity was normalized to the control of cells only.

2.16. May-Grünwald Giemsa staining and imaging.

Following microparticle treatment, medium was removed, and wells were rinsed 3x with DPBS, then cells were fixed with 4% PFA and rinsed with DI water. Jenner Stain Working Solution was applied for 10 minutes followed by rinsing with DI water. Giemsa Stain Stock Solution was diluted by 1 drop per mL DI water and applied to the wells for 1 hour. Cells were rinsed with DI water, Acetic Acid 1% Aqueous, and again with water before imaging with a bright-field microscope.

2.17. Flow cytometry for in vitro studies.

Following microparticle treatment, RAW 264.7 macrophages were characterized by flow cytometry using the BD FACS Celesta™ flow cytometer and FCSalyzer software. Cells alone, fluorescent particles, and non-fluorescent particles alone were used as controls to ensure appropriate fluorescence compensation. The 561 nm laser was used to excite fluorescent rhodamine-labeled particles at 546 nm and fluorescence was detected utilizing

a 585/15 bandpass filter. The 405 nm laser was used to excite fluorescent dansylcadaverine-labeled particles at 335 nm and detected with the 525/50 bandpass filter. Doublets were excluded. Side scatter versus forward scatter comparison was utilized to identify single cells and particles. Fluorescence intensity versus forward scatter was used to identify cells with high and low particle association. The number of events in each population was then used to analyze the percent of particle association with cells.

2.18. Mouse studies.

All procedures were approved by the National Jewish Health Institutional Animal Care and Use Committee. Wild type C57BL/6J mice were originally obtained from Jackson Laboratory and were bred in-house. Male and female mice of age 8–12 weeks were used for all experiments. Mice were sedated with inhaled isoflurane and then microparticles were delivered directly into the trachea using a gel-load pipette tip modified to have a slight bend in the distal end. All instillations were given in a volume of 50 μL. Mice were treated with either 2.75 or 113 μg microparticles. For studies of acute inflammation, LPS was administered intratracheally at a dose of 2 μg in tandem with microparticles. Control mice received either PBS alone or microparticles alone. Twenty-four hours after receipt of microparticles and/or LPS, mice were euthanized with intraperitoneal pentobarbital. The necks of mice were dissected to reveal the trachea and an 18-gauge needle was inserted to a depth of 2.5 cm. Lung lavage was performed with five 1 ml aliquots of PBS supplemented with 5mM EDTA. The first aliquot was centrifuged to pellet cells at 300xg for 5 minutes and 800 μL of supernatant were removed for analysis of cytokines. An equal volume of PBS was added back to resuspend cells. Cells from the first aliquot were then pooled with the other aliquots from the same mouse and vortexed to ensure uniform suspension of cells.

2.19. Imaging of cells from Bronchoalveolar lavage (BAL).

Pooled BAL fluid (125 μL) from each mouse was removed and cytospins were prepared using a Shandon Cytospin 4 (Thermo Scientific). Cytospins were examined under a fluorescent microscope and images obtained with a 20x objective. Total cell counts of pooled lavage fluid were obtained using a MoxiZ Cell Counter (GeminiBio, West Sacramento, CA). Differential cell counts were obtained using light microscopy on cytospin samples and confirmed using flow cytometry as described below.

2.20. Flow cytometry for in vivo studies.

Lavage cells were pelleted by centrifugation (300xg for 5 minutes) and resuspended in 100 μL of complete buffer containing PBS with 0.3% bovine serum albumin, 0.3 mM EDTA, and monoclonal antibodies at a dilution of 1:200. Single stained samples were used to ensure appropriate fluorescence compensation. After staining, cells were washed twice and flow cytometry was performed using a LSR Fortessa (BD Biosciences). Analysis was performed using FlowJo (BD Biosciences). Cells were identified using forward-scatter and side-scatter and doublets were excluded. CD45 was used to identify leukocytes. Neutrophils were identified from the leukocyte gate using Ly6G and CD11b. Macrophages were identified using CD64 and CD88 and further categorized into resident alveolar macrophages (Siglec-F high, CD11b low) and recruited monocyte derived macrophages (Siglec-F low, CD11b high).

2.21. Pro-inflammatory cytokines.

Enzyme-linked immunosorbent assays (ELISA) were performed to quantify production of IL-6 and TNF-α inflammatory cytokines in the culture media collected following different microparticle treatments.

2.22. Statistical Analysis.

The data analysis for this paper was generated using the Real Statistics Resource Pack software (Release 7.6). Copyright (2013 – 2021) Charles Zaiontz. www.real-statistics.com. Parametric data were confirmed by the Shapiro-Wilks and Levene's tests and then subjected to one-way or two-way ANOVA followed by Tukey's post-hoc analysis. For two-way ANOVA, if the interaction was significant, one-way ANOVA or t-test was performed. For non-parametric data, the data were analyzed by Kruskal-Wallis test followed by Pairwise Mann-Whitney test. The confidence level was α=.05. Normal distributions of microparticle diameters were fit in MATLAB with the fitdist() function. Statistical significance was set at $p<.05$. Data are reported as mean with standard deviation shown parenthetically in the text or as error bars in the graphs.

3.   RESULTS

3.1.   Characterization of thiol-acrylate microparticles.

Microparticles were synthesized by step-growth dispersion polymerization (Figure 1a) between the hexafunctional thiol monomer DPHMP and tetrafunctional acrylate monomer DTPTA (Figure 1b). The reaction was carried out off-stoichiometry with molar ratios of 1:1.20 and 1:1.33 of thiol:acrylate functional groups to form particles with 33% excess sulfhydryl or acrylate groups at the terminal ends, respectively. Using the same monomer concentration of 1 wt% in the polymerization reaction, SEM images revealed spherical microparticles with highly uniform shape and size. The particle diameters were 2.5(0.2) μm and 2.3(0.1) μm for the excess sulfhydryl and acrylate microparticles, respectively (Figure 1c). Their polydispersity indices were 0.0064 and 0.0019, respectively, which indicated monodisperse particles. Quantification of free thiols measured by absorbance indicated an increase ($p<.001$) in free thiols with increasing microparticle concentration for the excess sulfhydryl microparticles, confirming their presence (Figure 1d). For the excess acrylate microparticles, absorbance was lower ($p<.05$) than the excess thiol microparticles and below 0.2 for all microparticle concentrations (Figure 1d). There was a significant effect ($p<.001$) with microparticle concentration for the excess acrylate particles, resulting in small but significant higher absorbances with 8 and 16 mg/ml concentrations over the buffer. FTIR spectra confirmed the presence of the sulfhydryl-associated peak at 2550 cm^{-1} in the excess thiol particles and the acrylate peak at 810 cm^{-1} in the excess acrylate particles (Figure 1e). The acrylate peak was missing in the excess thiol particles and vice versa, further confirming both reactions. Zeta potential revealed differences in the excess thiol and excess acrylate particles as a function of pH (Figure 1f). Both particles had a zeta potential around −5 mV between pH 3 and 6, which suggested that the particles were predominantly neutral. With increasing pH, the excess thiol particles exhibited an increasingly negative zeta potential, reaching −20 mV at pH 9, which is attributed to the formation of a thiolate anion and consistent with the predicted pKa value of 8.8 for DPHMP (per manufacturer). The zeta

potential for the excess acrylate particles showed a similar trend, but the zeta potential was significantly less negative (i.e., −12 mV at pH 9). As a control, the excess thiols were reacted with methylmaleimide to cap the thiols. The zeta potential for the methyl-capped thiols was less negative when compared to the excess thiols, further confirming that that the presence of thiols contributed to the negative zeta potential at high pH.

3.2. Tunning microparticle size.

Microparticle size was varied by synthesizing 20% excess thiol particles with increasing monomer concentration from 0.4 to 15 wt% during the polymerization to form the particles. Representative SEM images and corresponding particle diameters presented as histograms (bin size = 0.01 μm) are shown in Figure 2a for each concentration. The mean diameter increased (p<.001) with increasing monomer concentration from 1 to 10 wt% and did not increase further with 12.5 and 15 wt% (Figure 2b). The polydispersity index (PDI) was less than 0.1 for all concentrations from 0.4 to 10 wt%, indicating monodisperse particles (Figure 2c). The PDI was much greater than 0.1 for 12.5 and 15 wt%, indicating polydisperse microspheres, which is consistent with the SEM images (Figure 2a). These results demonstrate that monodisperse DPHMP-DTPTA microparticles with diameters ranging from 0.8 to 7.4 μm were achieved.

3.3. Stability of microparticles as a function of pH.

In this experiment, microparticles were synthesized with either 20% excess acrylate (Figure 3a,b) or 20% excess thiol (Figure 3c,d) at 1 wt% monomer concentration. The stability of the microparticles at physiological pH and acidic pHs relevant to the phagosomal environment was analyzed by measuring the particle diameters over 14 days. Microparticles retained their spherical shape with no apparent changes to their morphology (Figure 3b,c). Particle diameter was affected by time (p<.001), but there were no obvious trends. Comparing the mean diameters from day 0 to day 14, the change in diameters was less than 2%. Diameters decreased (p<.001) with increasing pH for both excess thiol and excess acrylate particles, but the change was less than 1.5%. Taken together, these results indicate that the particles were stable across a pH range from 4 to 7 over two weeks.

3.4. Microparticle functionalization with amide and carboxyl groups.

The 33% excess thiol particles were reacted with iodoacetamide to form amide-functionalized particles (Figure 4a). FTIR confirmed the disappearance of the sulfhydryl-associated FTIR peak at 2550 cm^{-1} (Figure 4a). Quantifying the presence of free thiols showed a lower (p=.03) absorbance with the amide-functionalized particles compared to the 33% excess thiol particles at all concentrations (Figure 4a), confirming the thiols had reacted. There was a significant effect (p<.001) with microparticle concentration for amide-functionalized particles resulting in small, but significantly higher absorbance for the 16 mg/ml concentration when compared to the buffer. The diameter (n=300) of the amide-functionalized particles was 2.3(0.1) μm with a PDI of 0.00189, confirming that monodispersity was maintained. Zeta potentials of the amide-functionalized particles were compared to the sulfhydryl particles in buffers at pH 5 and 7 and filtered DI water at a particle concentration of 4 mg/mL (Figure 4b). At pH 5, the zeta potential was less negative for the sulfhydryl particles. With increasing pH, both particles were more negative at pH

7 with the sulfhydryl becoming increasingly more negative over the amide-functionalized particles. In DI water, both particles exhibited an even more negative zeta potential, which is attributed to the lack of charge shielding in water, with the sulfhydryl particle being the most negative. The mass swelling ratios of thiol and amide particles in DI water were not significantly different (Figure 4c).

The 33% excess acrylate particles were reacted with 3-mercaptopropionic acid to form carboxyl-terminated particles (Figure 4d). The reaction was monitored over time and acrylate conversion was calculated from disappearance of the 810 cm^{-1} acrylate peak (Figure 4d). The reaction was followed for two reaction conditions with 1 and 2% (g/v) 3-mercaptopropionic acid. Both reactions showed similar conversions over time, reaching 50% conversion after 24 hours and >90% conversion by 72 hours. The diameter (n=300) of the carboxyl-functionalized particles was 2.3(0.1) μm with a PDI of 0.00189, confirming that monodispersity was maintained. The zeta potentials of acrylate and carboxyl-functionalized particles were analyzed in buffers of pH 5 and 7 as well as filtered DI water at a particle concentration of 4 mg/mL (Figure 4e). At both pHs, the zeta potential for both particles was around –5 mV. In DI water, the zeta potential was more (p=.02) negative for the carboxyl-terminated particles compared to the acrylate particles, which is attributed to the negative charges of the carboxyl groups. The mass swelling ratio for carboxyl-terminated particles was significantly (p<.001) higher than that of acrylate particles in DI water.

3.5. Time-dependent effects of microparticles on RAW 264.7 macrophages.

RAW 264.7 macrophages were treated with 1.9 μm amide-terminated microparticles (55 μg/mL, equivalent to 145 particles/cell) with and without LPS stimulation (1 μg/mL) for 6 and 24 hours and assessed by metabolic activity, pro-inflammatory cytokine production, and uptake (Figure 5). Metabolic activity was used as an indicator of cell number to assess whether the microparticles impacted cell viability and/or cell proliferation. Metabolic activity was normalized to the control cells without microparticles and LPS at each respective time point (Figure 5a). For all experimental groups at both time points, metabolic activity was either maintained or enhanced. Metabolic activity was enhanced with LPS (p<.001) by 1.8-fold at 6 hours and 1.5-fold (p<.001) at 24 hours. At 6 hours, metabolic activity was not affected by the presence of microparticles but was elevated (p<.001) by 1.3-fold with both microparticles and LPS. After 24 hours, metabolic activity was 1.9-fold higher (p<.001) with microparticles compared to the control but was 20% lower (p=.02) with LPS. IL-6 and TNF-α production increased (p>.01) with LPS stimulation but were not affected by microparticles (Figure 5b,c). For LPS-stimulated macrophages, IL-6 production was not affected by microparticles, while TNF-α production was lower (p<.001) at 6 hours and then reached similar levels to the LPS only condition by 24 hours. Macrophages were treated with fluorescently labeled microparticles and assessed by flow cytometry. Representative dot plots show cells only, fluorescently labeled microparticles only, and then cells when treated with microparticles with and without LPS for 6 or 24 hours (Figure 5d). At 6 hours, 30% of macrophages without LPS treatment were associated with particles, which increased (p<.001) to 49% with LPS treatment. At 24 hours, those values increased (p=.004 and p<0.001) to 57% and 91% for macrophages without and with LPS stimulation, respectively (Figure 5e). Overall, these results indicate that 1.9 μm

amide-terminated microparticles do not negatively impact metabolic activity of macrophages nor do they induce an inflammatory response. Macrophage particle association increased with culture time and to a greater extent when stimulated with LPS.

3.6. Size-dependent effects of microparticles on RAW 264.7 macrophages.

RAW 264.7 cells were treated with 1.9 μm, 4.2 μm, and 8.1 μm (PDI = 0.004, 0.0007, and 0.026, respectively) amide-terminated microparticles (55 μg/mL, equivalent to 145, 13, and 2 particles/cell) with and without LPS stimulation (1 μg/mL) for 24 hours and assessed by metabolic activity, pro-inflammatory cytokine production, and uptake (Figure 6). The 1.9 μm microparticle data is the same data presented in Figure 5. Metabolic activity was assessed relative to control cells without microparticles and LPS (Figure 6a). For all experimental groups at both time points, metabolic activity was either maintained or enhanced. Metabolic activity was higher ($p < 0.01$) in unstimulated macrophages for all particle sizes compared to the control. The 1.9 μm particles had the highest metabolic activity relative to the other particle sizes. When stimulated with LPS, metabolic activity was not affected by the presence of microparticles or by their size (Figure 6a).

IL-6 and TNF-α production levels were normalized to the respective controls of cells only without or with LPS to account for slight differences in the cytokine levels from different experiments, where each experiment had its own no LPS and LPS controls. For unstimulated macrophages, IL-6 and TNF-α production were normalized to the unstimulated macrophages without microparticles (i.e., cells only). For stimulated macrophages, IL-6 and TNF-α production were normalized to the stimulated macrophages without microparticles (i.e., cells only). Normalized IL-6 production for unstimulated macrophages was not affected ($p = .10$) by particle size (Figure 6b). With LPS stimulation, absolute IL-6 production levels were significantly higher ($p < .002$) when compared to unstimulated macrophages for each experimental condition. Comparing normalized IL-6 production for the LPS stimulated macrophages, there was no effect ($p = .10$) with particle size. For unstimulated macrophages, normalized TNF-α production was higher ($p = .02$) for particle diameters of 4.2 μm and 8.1 μm compared to 1.9 μm particles (Figure 6c). With LPS stimulation, absolute TNF-α production levels were significantly higher ($p < .002$) when compared to unstimulated macrophages for each experimental condition. However, comparing normalized TNF-α production for the LPS stimulated macrophages, there was no effect ($p = .34$) with particle size.

Macrophages treated with microparticles were stained with May-Grünwald and imaged by bright-field microscopy and a black and white camera (Figure 6d). For unstimulated macrophages, 1.9 and 8.1 μm microparticles were visible within cells, indicating phagocytotic uptake. For the 4.2 μm particles, particles appeared attached to the macrophages but not internalized. On the contrary, for the stimulated macrophages, microparticle internalization was visible for all three particle sizes. The extent of particle association (binding and/or uptake) was analyzed by flow cytometry. For unstimulated cells, there was a decrease ($p < .001$) in particle association with increasing particle size with 57%, 29%, and 5.5% of macrophages with particles for the 1.9, 4.2, and 8.1 μm diameters. For

stimulated macrophages, greater than 90% of macrophages were with particles with no effect (p=.051) on particle size (Figure 6e).

3.7. Chemistry-dependent effects of microparticles on RAW 264.7 macrophages.

RAW 264.7 macrophages were treated with amide, carboxyl, and thiol-terminated microparticles with and without LPS stimulation (1 μg/mL) for 24 hours and assessed by metabolic activity, pro-inflammatory cytokine production, and uptake (Figure 7). Amide and thiol-terminated particles had an average diameter of 1.9 μm with a PDI of 0.004. Carboxyl particles had an average diameter of 1.6 μm and PDI of 0.002. Diameters were determined by analysis of SEM images (n=300). The 1.9 μm amide-terminated microparticle data are the same data presented in Figure 5 and Figure 6. Metabolic activity was assessed relative to control cells without microparticles and LPS (Figure 7a). For all experimental groups at both time points, metabolic activity was either maintained or enhanced. Metabolic activity was highest (p<.001) with the amide-terminated microparticles, whereas the metabolic activity was not affected by the carboxyl or thiol-terminated microparticles in unstimulated macrophages. When stimulated with LPS, metabolic activity was not affected by microparticle chemistry (Figure 7a).

Similar to Figure 6, IL-6 and TNF-α production levels were normalized to the respective controls of cells only without or with LPS to account for slight differences in the cytokine levels from different experiments, where each experiment had its own no LPS and LPS controls. Normalized IL-6 production for unstimulated and stimulated macrophages was not affected (p=.08 and p=.07, respectively) by particle chemistry (Figure 7b). With LPS stimulation, absolute IL-6 production levels were significantly higher (p<.002) when compared to unstimulated macrophages for each experimental condition. For unstimulated macrophages, normalized TNF-α production was higher (p=.02) for the carboxyl and thiol-terminated microparticles compared to the amide-terminated microparticles (Figure 7c). With LPS stimulation, absolute TNF-α production levels were significantly higher (p<.002) when compared to unstimulated macrophages for each experimental condition. Comparing the normalized TNF-α production for the stimulated macrophages, the carboxyl-terminated microparticle levels were significantly higher (p=.002) than those for the amide and thiol-terminated microparticles.

The extent of particle association (binding and/or uptake) was analyzed by flow cytometry. For unstimulated cells, microparticle chemistry affected (p<.001) particle association (Figure 7d). Amide-terminated microparticles had the lowest association at 57%, followed by thiol-terminated at 81% and then carboxyl-terminated at 95%. Particle association increased (p<.001) for the amide-terminated and the carboxyl-terminated microparticles. There was no effect of particle chemistry on particle association with stimulated macrophages (Figure 7d).

3.8. Microparticle treatment of human alveolar macrophages in vitro and mice lungs in vivo.

Human alveolar macrophages were treated with 1.9 μm amide-terminated microparticles (55 μg/mL, equivalent to 35 particles/cell) with or without LPS (1 μg/mL) for 6 and 24

hours *in vitro* and assessed by metabolic activity and pro-inflammatory cytokine production (Figure 8a,b). Metabolic activity was assessed relative to control cells without microparticles and LPS at each respective time point (Figure 8a). For all experimental groups at both time points, metabolic activity of the human alveolar macrophages was either maintained or enhanced. LPS did not impact metabolic activity of the macrophages at 6 hours but led to 1.6-fold increase (p=.02) at 24 hours. At 6 hours, metabolic activity was enhanced by 1.25-fold (p=.02) with microparticles but was 20% lower (p=.01) with LPS. At 24 hours, microparticle treatment did not impact human alveolar macrophage metabolic activity with or without LPS. IL-6 production increased (p>.05) with LPS stimulation at 6 and 24 hours but was not affected by microparticles (Figure 8b). Similar findings were observed for TNF-α production (Figure 8c).

Next, mice were treated with the same microparticles at doses of 2.75 and 113 μg particles per mouse via intratracheal delivery. BAL fluid was evaluated for IL-6 and TNF-α. The levels of both cytokines were elevated (p>.05) in control mice treated with LPS. However, when treated with particles at either concentration, no significant inflammatory response was observed (Figure 8d). Flow cytometry was performed to assess neutrophil recruitment as a sign of inflammation when treated with microparticles. Representative dot plots show Ly6G⁻ and Ly6G⁺ cells for controls with PBS and LPS and with microparticles at the two concentrations (Figure 8e). From the dot plots, neutrophil frequency was quantified. Neutrophil frequency was elevated (p=.01) in the control mice treated with LPS. However, minimal neutrophils were detected in the mice treated with microparticles at both concentrations, similar to the PBS control. Representative cytospin images from the BAL fluid show murine alveolar macrophages without any presence of neutrophils (Figure 8f). Due to autofluorescence of the alveolar macrophages, it was not possible to evaluate macrophages with particles by flow cytometry. However, the cytospin images show visible internalized particles within the alveolar macrophages (Figure 8f).

4. DISCUSSION

Monodisperse microparticles formed by a thiol-Michael addition polymerization reaction of the DTPTA-DPHMP system were fabricated over a range of sizes and readily functionalized with different chemistries. The particles were cyto-compatible and, depending on size and functionalization, were non-inflammatory. RAW 264.7 macrophage particle uptake was dependent on size and terminal functionality of the particles, as well as treatment time. Specifically, microparticle uptake by unstimulated cells was highest with 1.9 μm particles and particles functionalized with carboxyl-terminated groups. When activated by LPS, macrophages readily phagocytosed microparticles regardless of size or chemistry. Towards clinical translation of these microparticles for lung applications, microparticles delivered to human alveolar macrophages were cyto-compatible and non-inflammatory and, when delivered to mice intratracheally, were taken up by alveolar macrophages without inducing an inflammatory response. Overall, the study demonstrates that monodisperse microparticles formed by a thiol-Michael addition polymerization reaction are a promising therapeutic delivery platform to target macrophages for lung and other applications.

The microparticles synthesized via dispersion polymerization produce monodisperse microparticles with tunable size. Dispersion polymerization achieves monodisperse spherical microparticles with diameters in a range (i.e., 0.5–10 μm)[31] that is suitable for targeting macrophages.[20] Monodispersity is achieved through a homogenous nucleation step that occurs at low conversion in a single phase. When the chains reach a critical length or size, they become insoluble and precipitate, forming two phases. The polymerization then proceeds in a two-phase system until the reaction is complete.[42] Herein, particle size was controlled by monomer concentration, which led to increasing particle diameter consistent with other reports.[38] Monodispersity, defined by a PDI of less than 0.1, was achieved for monomer concentrations up to 10 wt%. Beyond 10 wt%, the particles were polydisperse. To this end, the surfactant and solvent characteristics are critically important to achieve monodisperse particles.[43] High functionality monomers can lead to poorer solubility at lower conversions, while high monomer concentrations can lead to increased probability of particle-particle reactions at low conversion; both have been shown to lead to polydisperse microparticles.[38] We surmise that the combination of these factors contributed to the formation of polydisperse microparticles when higher monomer concentrations were used. Further optimization of the surfactant and/or solvent would be needed to reduce polydispersity at the higher monomer concentrations.[43] Based on these findings, subsequent cell studies were limited to monodisperse microparticle formulations (i.e., 10 wt% monomer).

The DTPTA-DPHMP microparticles produce monodisperse microparticles with tunable chemistry. Thiol-Michael addition click chemistry was utilized to prepare microparticles with different chemistries by polymerizing off-stoichiometry. Microparticles were readily synthesized with excess thiols or excess acrylates that enabled a second reaction step to create functionalized microparticles. Herein, microparticles had terminal functionalities with a neutral moiety (i.e., amide-terminated), a negatively charged moiety (i.e., carboxyl-terminated), or a sulfhydryl (i.e., excess thiol particles). At neutral or acidic pH, the base chemistry of the particles was close to neutral, which is consistent with reports of other particles (e.g., polystyrene) functionalized with neutral groups.[44] With the presence of either sulfhydryl or carboxyl groups, the particles at pH 7 were more negative than the amide functionalized particles, which is attributed to the formation of a thiolate anion[45] or carboxylic acid, respectively. In the presence of serum, the differences in surface charge can impact the types of proteins that adsorb and opsonize the particles.[46] However, at acidic pHs (4–5) relevant to the phagosome, the particles were close to neutral due to their pKa's, showing minimal differences in surface charge among the different particle chemistries. Thus, the particles in the extracellular environment may interact differently with macrophages depending on particle chemistry; once phagocytosed, differences in particle chemistry may have less of an effect.

The microparticles are stable across physiological and acidic pHs up to two weeks. The DTPTA-DPHMP network has an ester bond within the crosslinks that is susceptible to hydrolysis. The ester bond is also adjacent to a sulfur atom, which has been shown to increase the rate of hydrolysis for esters.[47] Ester bonds are also known to undergo acid-catalyzed hydrolysis.[48] Despite the chemistry and acidic pH, degradation was minimal over the course of two weeks. Degradation occurred within minutes under accelerated conditions

by a base-catalyzed hydrolysis reaction, confirming that the microparticles are indeed degradable. The slow degradation observed in this study is attributed to a highly crosslinked network due to the low molecular weight and high functionality of the monomers. The highly crosslinked network is evident in part by the low degree of swelling in water (i.e., volumetric swelling ratios of 1.5–2.5). Moreover, functionalizing the particles with carboxylic acid resulted in a significant, although modest increase in swelling (i.e., 1.5 to 2.5), which can be attributed to the highly crosslinked nature of the particles. Depending on the application, future studies could explore alternative formulations that result in lower crosslink density (e.g., lower thiol-acrylate ratio) and/or different chemistries to increase rate of degradation and/or rate of hydrolysis. In the current study, the use of stable microparticles at physiological and phagosomal pHs was important to study the impact of the microparticle size and functionality on macrophage phagocytosis, without complicating the findings due to particle degradation.

RAW 264.7 macrophages phagocytose the microparticles in a time and size-dependent manner. Using the amide functionalized 1.9 μm particles, microparticle uptake nearly doubled from 6 to 24 hours without eliciting an inflammatory response. Similar results were reported for PLGA microparticles of similar size where phagocytosis increased from 30% to 65% from 4 to 24 hours.[49] Phagocytosis relies initially on the recognition and attachment of the microparticle to the cell membrane followed by internalization. The first step is thought to be the rate limiting step to uptake.[12] The 1.9 μm amide-terminated microparticles led to the greatest uptake by RAW 264.7 macrophages when compared to 4.2 and 8.1 μm microparticles of the same chemistry. Champion *et al.*[12] showed that with polystyrene microparticles ranging in diameter from 0.9 to 9 μm, phagocytosis was the highest for particles with diameters of 2–3 μm. The authors posited that this size is optimal because the particles can fit within the membrane ruffles of macrophages, resulting in greater contact area between the particle and the cell membrane – thus facilitating phagocytosis. In the current study, with increasing particle diameter from 1.9 to 8.1 μm, uptake was significantly decreased, which is consistent with other studies.[4,12,50] We observed macrophages with internalized 4.0 and 8.1 μm microparticles, confirming that they can phagocytose microparticles of these sizes. Studies have suggested an upper limit for phagocytosis of spherical particles to be on the size of a macrophage or around 10 μm.[51] Since phagocytosis depends on rate of attachment,[12] we surmise that the decrease in uptake with larger particles is due to weakly attached particles. Interestingly, TNF-α levels were significantly higher for the 4.0 and 8.1 μm microparticles. Studies have suggested that microparticles, when attached to the cell membrane but not phagocytosed, can induce a pro-inflammatory response; this was observed for 6.5 μm PLGA microparticles.[14] Because the experiments were performed in the presence of FBS, serum proteins will adsorb to the particles.[46] Surface adsorbed proteins can bind and activate cell surface receptors, such as Toll-like receptors, which recognize damage-associated molecular patterns (DAMPs) to induce pro-inflammatory cytokine production but which are not directly involved in phagocytosis.[52,53] Taken together, we conclude that when microparticles strongly attach to cell membrane (i.e., 1.9 μm) they are readily phagocytosed and minimize an inflammatory response while weakly attached (i.e., larger) particles have lower rates of internalization and instead elicit an inflammatory response.

The chemistry of the microparticles impacts the extent of particle uptake by RAW 264.7 macrophages. Thiol and carboxyl terminated microparticles led to significantly greater uptake over the more neutral amide microparticles. Several studies have reported that higher surface charge (negative or positive) increases particle uptake.[4,17,54,55] This can be attributed to differences in the surface adsorbed proteins, where the type of protein and strength of the adsorption depends on the surface chemistry. FBS contains several specific and non-specific opsonizing factors (e.g., immunoglobulin G, fibronectin, vitronectin)[53] that, if adsorbed to particles, would significantly increase uptake.[54] While the thiol functionalized particles are negatively charged at physiological pH and could impact the type of adsorbed proteins, the free thiols are highly reactive. Previous studies have shown that thiolated monomers can react with cells through cell surface free thiols.[56] Thus, we hypothesize that the high rate of uptake with the thiolated microparticles relative to the amine-terminated microparticles could also be attributed to their reaction with membrane free thiols on macrophages. Interestingly, the carboxyl and thiol terminated microparticles elicited an inflammatory response, while the amide microparticles did not. It is possible that the type of serum proteins that adsorb to the microparticles could have led to more DAMPs for the carboxyl and thiol-terminated microparticles. Moreover, the type of opsonin will influence whether inflammatory cytokines are produced during phagocytosis.[53] In summary, these findings show that for the microparticles, the terminal functional group significantly impacts the extent of phagocytosis and the production of pro-inflammatory cytokines.

Microparticles have been used to deliver anti-inflammatory drugs to macrophages.[10] Thus, it was important to assess whether the microparticles would be taken up by pro-inflammatory macrophages. Indeed, activated macrophages readily phagocytose microparticles regardless of particle size and chemistry. Pro-inflammatory cytokines such as TNF-α can enhance phagocytosis capabilities of phagocytic cells,[57] but high levels are often inhibitory.[58] Macrophages are known to undergo endotoxin tolerance with continued exposure to endotoxins like LPS, causing a switch to an immunosuppressive phenotype with enhanced phagocytic capabilities.[59,60] Our group has previously reported that macrophages when interacting with a biomaterial and exposed to LPS transition to an alternatively activated M2-like phenotype within 24 hours.[61] Thus, it is possible that the high level of LPS treatment, which simulates the initial inflammatory response, is subsequently followed by a transition to a macrophage phenotype with greater phagocytic capabilities; this process is similar to that observed during an infection.[59] Our findings differ from a study that examined 0.6 μm particles prepared from p(N-isopropylacrylamide-co-acrylic acid) where naïve RAW 264.7 macrophages showed higher uptake when compared to LPS-stimulated macrophages.[62] One difference from our study was that the authors stimulated the macrophages with LPS for 24 hours, removed the medium, and then treated the cells with microparticles for four hours. The difference may be due to the role that receptors for LPS (i.e., TLR4) play in modulating opsonin and nonopsonin receptors during phagocytosis.[59] It is interesting to note that in the presence of LPS, TNF-α production was highest for the carboxyl-terminated particles, indicating that these particles were able to induce an even greater inflammatory response over LPS alone. This finding is consistent with other studies that reported elevated pro-inflammatory cytokine levels when opsonized particles were combined with LPS[63] and further points to the role that adsorbed serum proteins play in

inducing an inflammatory response and in facilitating particle phagocytosis. Taken together, these findings indicate that either activated macrophages or LPS-coated microparticles lead to rapid microparticle internalization and is independent of particle properties (i.e., size and chemistry).

The microparticles are noninflammatory and readily taken up by alveolar macrophages. Of critical importance in the context of the lung are particulate delivery systems capable of reaching alveolar macrophages, cells that reside in the lungs and play an extensive role in regulating the immune response to inflammatory triggers.[64–68] Since the airway diameter limits the maximum deliverable microparticle size to the alveoli where these macrophages reside, 1.9 μm particles were chosen for studies in human alveolar macrophages *in vitro* and mouse lungs *in vivo*. Moreover, the amide-terminated functionalized microparticles were chosen because they did not elicit an inflammatory response in RAW 264.7 macrophages. Cytospins of BAL fluid from *in vivo* experimentation demonstrated that this particle size was successful in reaching and being taken up by alveolar macrophages in mouse lungs. Microparticles are also known to be inflammatory mediators in lung disease,[69] thus it was important to assess if the microparticles induce inflammation in alveolar macrophages. In human alveolar macrophages, the microparticles did not evoke IL-6 or TNF-α pro-inflammatory cytokine production, nor did intratracheal microparticle delivery in mice. Importantly, very little neutrophil recruitment was observed *in vivo*. In all, DTPTA-DPHMP microparticles show promise for lung-specific applications due to their tunable size and non-inflammatory nature.

5. CONCLUSION

In summary, this study demonstrates monodisperse microparticles formed from the thiol-Michael addition polymerization reaction of the DTPTA-DPHMP system with highly tunable sizes and which can be functionalized with different chemistries to impact particle surface properties. Macrophage uptake of particles was dependent on size and chemistry for naïve (i.e., unstimulated) RAW 264.7 macrophages, while LPS stimulated macrophages rapidly phagocytosed microparticles regardless of size and chemistry. While amide-terminated microparticles resulted in reduced uptake, they did not induce an inflammatory response in macrophages. Carboxyl- and thiol- terminated microparticles led to much higher rates of uptake but were compromised by elevated immune responses. Taken together, our findings suggest that amide-terminated microparticles in the range of 2 μm in diameter are promising to investigate their potential as therapeutic delivery vehicles for targeting alveolar macrophages in lung applications.

ACKNOWLEDGMENT

ABBREVIATIONS

ATR	Attenuated Total Reflection
DMEM	Dulbecco's Modified Eagle's Medium
DMSO	dimethyl sulfoxide
DPBS	Dulbecco's phosphate buffered saline
DPHMP	dipentaerythritol hexa-3-mercaptopropionate
DTPTA	di(trimethylolpropane) tetraacrylate
EDTA	ethylenediaminetetraacetic acid
ELISA	enzyme-linked immunosorbent assay
FBS	fetal bovine serum
FTIR	Fourier Transform Infrared
HCl	hydrochloric acid
IL-6	interleukin 6
LPS	lipopolysaccharide
MeHQ	4-methoxyphenol
NaOH	sodium hydroxide
OPA	o-Phthaldialdehyde
PVP	polyvinylpyrrolidone
SEM	Scanning Electron Microscope
TEA	triethylamine
TLR4	Toll-like receptor 4
TNF-α	tumor necrosis factor alpha

REFERENCES

(1). Xiong M-H; Bao Y; Yang X-Z; Zhu Y-H; Wang J Delivery of Antibiotics with Polymeric Particles. Advanced Drug Delivery Reviews 2014, 78, 63–76. 10.1016/j.addr.2014.02.002. [PubMed: 24548540]

(2). Yawalkar AN; Pawar MA; Vavia PR Microspheres for Targeted Drug Delivery- A Review on Recent Applications. Journal of Drug Delivery Science and Technology 2022, 75, 103659. 10.1016/j.jddst.2022.103659.

(3). Koerner J; Horvath D; Groettrup M Harnessing Dendritic Cells for Poly (D,L-Lactide-Co-Glycolide) Microspheres (PLGA MS)—Mediated Anti-Tumor Therapy. Front. Immunol 2019, 10, 707. 10.3389/fimmu.2019.00707. [PubMed: 31024545]

(4). Patel B; Gupta N; Ahsan F Particle Engineering to Enhance or Lessen Particle Uptake by Alveolar Macrophages and to Influence the Therapeutic Outcome. European Journal of Pharmaceutics and Biopharmaceutics 2015, 89, 163–174. 10.1016/j.ejpb.2014.12.001. [PubMed: 25497488]

(5). Mehta M; Deeksha; Sharma N; Vyas M; Khurana N; Maurya PK; Singh H; Andreoli de Jesus TP; Dureja H; Chellappan DK; Gupta G; Wadhwa R; Collet T; Hansbro PM; Dua K; Satija S Interactions with the Macrophages: An Emerging Targeted Approach Using Novel Drug Delivery Systems in Respiratory Diseases. Chemico-Biological Interactions 2019, 304, 10–19. 10.1016/j.cbi.2019.02.021. [PubMed: 30849336]

(6). Ruirui Z; He J; Xu X; Li S; Peng H; Deng Z; Huang Y PLGA-Based Drug Delivery System for Combined Therapy of Cancer: Research Progress. Mater. Res. Express 2021, 8 (12), 122002. 10.1088/2053-1591/ac3f5e.

(7). Richards DM; Endres RG The Mechanism of Phagocytosis: Two Stages of Engulfment. Biophysical Journal 2014, 107 (7), 1542–1553. 10.1016/j.bpj.2014.07.070. [PubMed: 25296306]

(8). Yue H; Wei W; Yue Z; Lv P; Wang L; Ma G; Su Z Particle Size Affects the Cellular Response in Macrophages. European Journal of Pharmaceutical Sciences 2010, 41 (5), 650–657. 10.1016/j.ejps.2010.09.006. [PubMed: 20870022]

(9). Hirota K; Hasegawa T; Nakajima T; Inagawa H; Kohchi C; Soma G-I; Makino K; Terada H Delivery of Rifampicin–PLGA Microspheres into Alveolar Macrophages Is Promising for Treatment of Tuberculosis. Journal of Controlled Release 2010, 142 (3), 339–346. 10.1016/j.jconrel.2009.11.020. [PubMed: 19951729]

(10). Wofford KL; Cullen DK; Spiller KL Modulation of Macrophage Phenotype via Phagocytosis of Drug-loaded Microparticles. J. Biomed. Mater. Res 2019, 107 (6), 1213–1224. 10.1002/jbm.a.36617.

(11). Wofford KL; Singh BS; Cullen DK; Spiller KL Biomaterial-Mediated Reprogramming of Monocytes via Microparticle Phagocytosis for Sustained Modulation of Macrophage Phenotype. Acta Biomaterialia 2020, 101, 237–248. 10.1016/j.actbio.2019.11.021. [PubMed: 31731024]

(12). Champion JA; Walker A; Mitragotri S Role of Particle Size in Phagocytosis of Polymeric Microspheres. Pharmaceutical Research 2008, 25 (8), 1815–1821. 10.1007/s11095-008-9562-y. [PubMed: 18373181]

(13). Thomas C; Gupta V; Ahsan F Particle Size Influences the Immune Response Produced by Hepatitis B Vaccine Formulated in Inhalable Particles. Pharm Res 2010, 27 (5), 905–919. 10.1007/s11095-010-0094-x. [PubMed: 20232117]

(14). Nicolete R; Santos D. F. dos; Faccioli LH The Uptake of PLGA Micro or Nanoparticles by Macrophages Provokes Distinct in Vitro Inflammatory Response. International Immunopharmacology 2011, 11 (10), 1557–1563. 10.1016/j.intimp.2011.05.014. [PubMed: 21621649]

(15). Jeon S; Clavadetscher J; Lee D-K; Chankeshwara S; Bradley M; Cho W-S Surface Charge-Dependent Cellular Uptake of Polystyrene Nanoparticles. Nanomaterials 2018, 8 (12), 1028. 10.3390/nano8121028. [PubMed: 30544753]

(16). Kim J; Chankeshwara SV; Thielbeer F; Jeong J; Donaldson K; Bradley M; Cho W-S Surface Charge Determines the Lung Inflammogenicity: A Study with Polystyrene Nanoparticles. Nanotoxicology 2015, 1–8. 10.3109/17435390.2015.1022887.

(17). Makino K; Yamamoto N; Higuchi K; Harada N; Ohshima H; Terada H Phagocytic Uptake of Polystyrene Microspheres by Alveolar Macrophages: Effects of the Size and Surface Properties of the Microspheres. Colloids and Surfaces B: Biointerfaces 2003, 27 (1), 33–39. 10.1016/S0927-7765(02)00042-5.

(18). Lee W-H; Loo C-Y; Traini D; Young PM Nano- and Micro-Based Inhaled Drug Delivery Systems for Targeting Alveolar Macrophages. Expert Opinion on Drug Delivery 2015, 12 (6), 1009–1026. 10.1517/17425247.2015.1039509. [PubMed: 25912721]

(19). Vlachopoulos A; Karlioti G; Balla E; Daniilidis V; Kalamas T; Stefanidou M; Bikiaris ND; Christodoulou E; Koumentakou I; Karavas E; Bikiaris DN Poly(Lactic Acid)-Based Microparticles for Drug Delivery Applications: An Overview of Recent Advances. Pharmaceutics 2022, 14 (2), 359. 10.3390/pharmaceutics14020359. [PubMed: 35214091]

(20). Hirota K; Hasegawa T; Hinata H; Ito F; Inagawa H; Kochi C; Soma G-I; Makino K; Terada H Optimum Conditions for Efficient Phagocytosis of Rifampicin-Loaded PLGA Microspheres by Alveolar Macrophages. Journal of Controlled Release 2007, 119 (1), 69–76. 10.1016/j.jconrel.2007.01.013. [PubMed: 17335927]

(21). Sun R; Liu X; Zhang Y; Li Q; Zhu Y; Fan C Size-Dependent Cellular Uptake and Sustained Drug Release of PLGA Particles. Particuology 2023, 73, 1–7. 10.1016/j.partic.2022.03.003.

(22). Sharma PR; Dravid AA; Kalapala YC; Gupta VK; Jeyasankar S; Goswami A; Agarwal R Cationic Inhalable Particles for Enhanced Drug Delivery to M. Tuberculosis Infected Macrophages. Biomaterials Advances 2022, 133, 112612. 10.1016/j.msec.2021.112612. [PubMed: 35527151]

(23). Liu Z; Li X; Xiu B; Duan C; Li J; Zhang X; Yang X; Dai W; Johnson H; Zhang H; Feng X A Novel and Simple Preparative Method for Uniform-Sized PLGA Microspheres: Preliminary Application in Antitubercular Drug Delivery. Colloids and Surfaces B: Biointerfaces 2016, 145, 679–687. 10.1016/j.colsurfb.2016.05.085. [PubMed: 27289309]

(24). Liu R; Ma G; Meng F-T; Su Z-G Preparation of Uniform-Sized PLA Microcapsules by Combining Shirasu Porous Glass Membrane Emulsification Technique and Multiple Emulsion-Solvent Evaporation Method. Journal of Controlled Release 2005, 103 (1), 31–43. 10.1016/j.jconrel.2004.11.025. [PubMed: 15710498]

(25). Sharma G; Valenta DT; Altman Y; Harvey S; Xie H; Mitragotri S; Smith JW Polymer Particle Shape Independently Influences Binding and Internalization by Macrophages. Journal of Controlled Release 2010, 147 (3), 408–412. 10.1016/j.jconrel.2010.07.116. [PubMed: 20691741]

(26). Sadhu RK; Barger SR; Peni S; Igli A; Krendel M; Gauthier NC; Gov NS A Theoretical Model of Efficient Phagocytosis Driven by Curved Membrane Proteins and Active Cytoskeleton Forces. Soft Matter 2023, 19 (1), 31–43. 10.1039/D2SM01152B.

(27). Mathaes R; Winter G; Besheer A; Engert J Influence of Particle Geometry and PEGylation on Phagocytosis of Particulate Carriers. International Journal of Pharmaceutics 2014, 465 (1), 159–164. 10.1016/j.ijpharm.2014.02.037. [PubMed: 24560647]

(28). Beningo KA; Wang YL Fc-Receptor-Mediated Phagocytosis Is Regulated by Mechanical Properties of the Target. Journal of Cell Science 2002, 115 (4), 849–856. [PubMed: 11865040]

(29). Kolb HC; Finn MG; Sharpless KB Click Chemistry: Diverse Chemical Function from a Few Good Reactions. Angewandte Chemie-International Edition 2001, 40 (11), 2004–2021. [PubMed: 11433435]

(30). Hoyle CE; Bowman CN Thiol-Ene Click Chemistry. Angewandte Chemie-International Edition 2010, 49 (9), 1540–1573. 10.1002/anie.200903924. [PubMed: 20166107]

(31). Goldmann AS; Barner L; Kaupp M; Vogt AP; Barner-Kowollik C Orthogonal Ligation to Spherical Polymeric Microparticles: Modular Approaches for Surface Tailoring. Progress in Polymer Science 2012, 37 (7), 975–984. 10.1016/j.progpolymsci.2011.11.008.

(32). Alimohammadi F; Wang C; Durham OZ; Norton HR; Bowman CN; Shipp DA Radical Mediated Thiol-Ene/Yne Dispersion Polymerizations. Polymer 2016, 105, 180–186. 10.1016/j.polymer.2016.10.016.

(33). Cai S; Weng Z; Zheng Y; Zhao B; Gao Z; Gao C High Porosity Microspheres with Functional Groups Synthesized by Thiol–Yne Click Suspension Polymerization. Polym. Chem 2016, 7 (48), 7400–7407. 10.1039/C6PY01824F.

(34). Barner L Synthesis of Microspheres as Versatile Functional Scaffolds for Materials Science Applications. Adv. Mater 2009, 21 (24), 2547–2553. 10.1002/adma.200900373.

(35). Hafeez S; Barner L; Nebhani L TEMPO Driven Mild and Modular Route to Functionalized Microparticles. Macromol. Rapid Commun 2018, 39 (19), 1800169. 10.1002/marc.201800169.

(36). Jiang K; Liu Y; Yan Y; Wang S; Liu L; Yang W Combined Chain- and Step-Growth Dispersion Polymerization toward PSt Particles with Soft, Clickable Patches. Polym. Chem 2017, 8 (8), 1404–1416. 10.1039/C6PY02094A.

(37). Liu Y; Wei M; Jiang X; Ren M; Liu L; Wen B; Yang W Anomalously Shaped Functional Particles Prepared by Thiol-Isocyanate Off-Stoichiometric Click Dispersion Polymerization. Langmuir 2020, 36 (47), 14417–14424. 10.1021/acs.langmuir.0c02798. [PubMed: 33198464]

(38). Wang C; Podgórski M; Bowman CN Monodisperse Functional Microspheres from Step-Growth "Click" Polymerizations: Preparation, Functionalization and Implementation. Mater. Horiz 2014, 1 (5), 535–539. 10.1039/C4MH00082J.

(39). Wang C; Zhang X; Podgorski M; Xi W; Stansbury J; Bowman CN Monodispersity/Narrow Polydispersity Cross-Linked Microparticles Prepared by Step-Growth Thiol-Michael Addition Dispersion Polymerizations. Macromolecules 2015, 48 (23), 8461–8470. 10.1021/acs.macromol.5b02146.

(40). Anderson AJ; Grey E; Bongiardina NJ; Bowman CN; Bryant SJ Synthesis and Characterization of Click Nucleic Acid Conjugated Polymeric Microparticles for DNA Delivery Applications. Biomacromolecules 2021, 22 (3), 1127–1136. 10.1021/acs.biomac.0c01563. [PubMed: 33621070]

(41). Hume PS; Gibbings SL; Jakubzick CV; Tuder RM; Curran-Everett D; Henson PM; Smith BJ; Janssen WJ Localization of Macrophages in the Human Lung via Design-Based Stereology. Am J Respir Crit Care Med 2020, 201 (10), 1209–1217. 10.1164/rccm.201911-2105OC. [PubMed: 32197050]

(42). Tuncel A; Kahraman R; Pi kin E Monosize Polystyrene Microbeads by Dispersion Polymerization. J. Appl. Polym. Sci 1993, 50 (2), 303–319. 10.1002/app.1993.070500212.

(43). Takahashi K; Miyamori S; Uyama H; Kobayashi S Preparation of Micron-Size Monodisperse Poly(2-Hydroxyethyl Methacrylate) Particles by Dispersion Polymerization. J. Polym. Sci. A Polym. Chem 1996, 34 (2), 175–182. 10.1002/(SICI)1099-0518(19960130)34:2<175::AID-POLA3>3.0.CO;2-T.

(44). Thielbeer F; Donaldson K; Bradley M Zeta Potential Mediated Reaction Monitoring on Nano and Microparticles. Bioconjugate Chem. 2011, 22 (2), 144–150. 10.1021/bc1005015.

(45). Shyue J-J; De Guire MR; Nakanishi T; Masuda Y; Koumoto K; Sukenik CN Acid–Base Properties and Zeta Potentials of Self-Assembled Monolayers Obtained via in Situ Transformations. Langmuir 2004, 20 (20), 8693–8698. 10.1021/la049247q. [PubMed: 15379494]

(46). Serda RE; Blanco E; Mack A; Stafford SJ; Amra S; Li Q Proteomic Analysis of Serum Opsonins Impacting Biodistribution and Cellular Association of Porous Silicon Microparticles. 2014.

(47). Rydholm AE; Anseth KS; Bowman CN Effects of Neighboring Sulfides and PH on Ester Hydrolysis in Thiol-Acrylate Photopolymers. Acta Biomaterialia 2007, 3 (4), 449–455. 10.1016/j.actbio.2006.12.001. [PubMed: 17276150]

(48). Wu L; Ding J Effects of Porosity and Pore Size Onin Vitro Degradation of Three-Dimensional Porous Poly(D,L-Lactide-Co-Glycolide) Scaffolds for Tissue Engineering. J. Biomed. Mater. Res 2005, 75A (4), 767–777. 10.1002/jbm.a.30487.

(49). Di J; Gao X; Du Y; Zhang H; Gao J; Zheng A Size, Shape, Charge and "Stealthy" Surface: Carrier Properties Affect the Drug Circulation Time in Vivo. Asian Journal of Pharmaceutical Sciences 2021, 16 (4), 444–458. 10.1016/j.ajps.2020.07.005. [PubMed: 34703494]

(50). Edwards DA; Hanes J; Caponetti G; Hrkach J; Ben-Jebria A; Eskew ML; Mintzes J; Deaver D; Lotan N; Langer R Large Porous Particles for Pulmonary Drug Delivery. Science 1997, 276 (5320), 1868–1872. 10.1126/science.276.5320.1868. [PubMed: 9188534]

(51). Baranov MV; Kumar M; Sacanna S; Thutupalli S; van den Bogaart G Modulation of Immune Responses by Particle Size and Shape. Front. Immunol 2021, 11, 607945. 10.3389/fimmu.2020.607945. [PubMed: 33679696]

(52). McKiel LA; Woodhouse KA; Fitzpatrick LE; Hall D The Role of Toll-like Receptor Signaling in the Macrophage Response to Implanted Materials. MRS Commun. 2020, No. 1, 55–68.

(53). Underhill DM; Ozinsky A Phagocytosis of Microbes: Complexity in Action. Annu. Rev. Immunol 2002, 20 (1), 825–852. 10.1146/annurev.immunol.20.103001.114744. [PubMed: 11861619]

(54). Roser M; Fischer D; Kissel T Surface-Modified Biodegradable Albumin Nano- and Microspheres. II: Effect of Surface Charges on in Vitro Phagocytosis and Biodistribution in Rats. European Journal of Pharmaceutics and Biopharmaceutics 1998, 46 (3), 255–263. 10.1016/S0939-6411(98)00038-1. [PubMed: 9885296]

(55). He C; Hu Y; Yin L; Tang C; Yin C Effects of Particle Size and Surface Charge on Cellular Uptake and Biodistribution of Polymeric Nanoparticles. Biomaterials 2010, 31 (13), 3657–3666. 10.1016/j.biomaterials.2010.01.065. [PubMed: 20138662]

(56). Chu S; Maples MM; Bryant SJ Cell Encapsulation Spatially Alters Crosslink Density of Poly(Ethylene Glycol) Hydrogels Formed from Free-Radical Polymerizations. Acta. Biomater 2020, 109, 37–50. 10.1016/j.actbio.2020.03.033. [PubMed: 32268243]

(57). Pechkovsky DV; Potapnev MP; Zalutskaya OM Different Patterns of Cytokine Regulation of Phagocytosis and Bacterial Killing by Human Neutrophils. International Journal of Antimicrobial Agents 1996, 7 (1), 33–40. 10.1016/0924-8579(96)00007-6. [PubMed: 18611733]

(58). Michlewska S; Dransfield I; Megson IL; Rossi AG Macrophage Phagocytosis of Apoptotic Neutrophils Is Critically Regulated by the Opposing Actions of Pro-inflammatory and Anti-inflammatory Agents: Key Role for TNF-α. FASEB j. 2009, 23 (3), 844–854. 10.1096/fj.08-121228. [PubMed: 18971259]

(59). Hortová-Kohoutková M; Tidu F; De Zuani M; Šrámek V; Helán M; Fri J Phagocytosis–Inflammation Crosstalk in Sepsis: New Avenues for Therapeutic Intervention. Shock 2020, 54 (5), 606–614. 10.1097/SHK.0000000000001541. [PubMed: 32516170]

(60). Biswas SK; Lopez-Collazo E Endotoxin Tolerance: New Mechanisms, Molecules and Clinical Significance. Trends in Immunology 2009, 30 (10), 475–487. 10.1016/j.it.2009.07.009. [PubMed: 19781994]

(61). Lynn AD; Bryant SJ Phenotypic Changes in Bone Marrow-Derived Murine Macrophages Cultured on PEG-Based Hydrogels Activated or Not by Lipopolysaccharide. Acta Biomaterialia 2011, 7 (1), 123–132. 10.1016/j.actbio.2010.07.033. [PubMed: 20674808]

(62). Wang D; Phan N; Isely C; Bruene L; Bratlie KM Effect of Surface Modification and Macrophage Phenotype on Particle Internalization. Biomacromolecules 2014, 15 (11), 4102–4110. 10.1021/bm5011382. [PubMed: 25268218]

(63). Ueno T; Yamamoto Y; Kawasaki K Phagocytosis of Microparticles Increases Responsiveness of Macrophage-like Cell Lines U937 and THP-1 to Bacterial Lipopolysaccharide and Lipopeptide. Sci Rep 2021, 11 (1), 6782. 10.1038/s41598-021-86202-5. [PubMed: 33762618]

(64). Allard B; Panariti A; Martin JG Alveolar Macrophages in the Resolution of Inflammation, Tissue Repair, and Tolerance to Infection. Front. Immunol 2018, 9, 1777. 10.3389/fimmu.2018.01777. [PubMed: 30108592]

(65). Puttur F; Gregory LG; Lloyd CM Airway Macrophages as the Guardians of Tissue Repair in the Lung. Immunol Cell Biol 2019, 97 (3), 246–257. 10.1111/imcb.12235. [PubMed: 30768869]

(66). Byrne AJ; Mathie SA; Gregory LG; Lloyd CM Pulmonary Macrophages: Key Players in the Innate Defence of the Airways. Thorax 2015, 70 (12), 1189–1196. 10.1136/thoraxjnl-2015-207020. [PubMed: 26286722]

(67). Watanabe S; Alexander M; Misharin AV; Budinger GRS The Role of Macrophages in the Resolution of Inflammation. Journal of Clinical Investigation 2019, 129 (7), 2619–2628. 10.1172/JCI124615. [PubMed: 31107246]

(68). Lee J-W; Chun W; Lee HJ; Min J-H; Kim S-M; Seo J-Y; Ahn K-S; Oh S-R The Role of Macrophages in the Development of Acute and Chronic Inflammatory Lung Diseases. Cells 2021, 10 (4), 897. 10.3390/cells10040897. [PubMed: 33919784]

(69). Mohning MP; Thomas SM; Barthel L; Mould KJ; McCubbrey AL; Frasch SC; Bratton DL; Henson PM; Janssen WJ Phagocytosis of Microparticles by Alveolar Macrophages during Acute Lung Injury Requires MerTK. American Journal of Physiology-Lung Cellular and Molecular Physiology 2018, 314 (1), L69–L82. 10.1152/ajplung.00058.2017. [PubMed: 28935638]
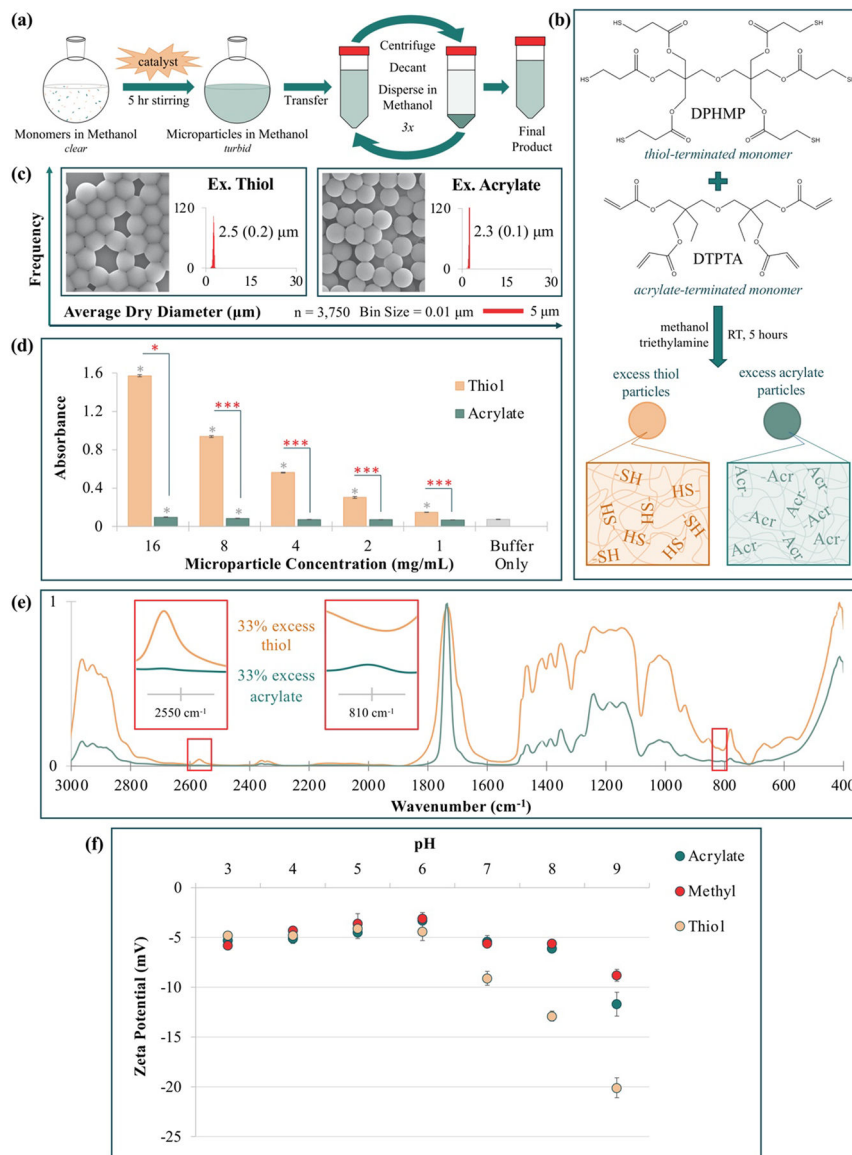
Figure 1.

(a) Microparticles were synthesized by dispersion polymerization and recovered by centrifugation. (b) Multi-arm thiol and acrylate monomers, DTPTA and DPHMP, were reacted off-stoichiometry to form particles with excess sulfhydryl or acrylate terminal chemistries. (c) Representative SEM images are provided along with histograms of diameter distribution (n=3,750, bin size = 0.01 μm), and mean (standard deviation). (d) Quantification of sulfhydryl groups as measured by absorbance using the Ellman's Assay as a function of microparticle concentration for 33% excess sulfhydryl and acrylate microparticles. Pairwise comparisons are shown by asterisks above a column for comparison from buffer or between the two microparticle types where * is p<0.05 and *** is p< 0.001. (e) FTIR spectra of excess acrylate particles (green) included an acrylate peak at 810 cm^{-1} while spectra of excess thiol particles (orange) had a thiol-associated peak at 2550 cm^{-1}. (f) Zeta potential of 33% excess sulfhydryl, 33% excess acrylate, and 33% excess sulfhydryl microparticles
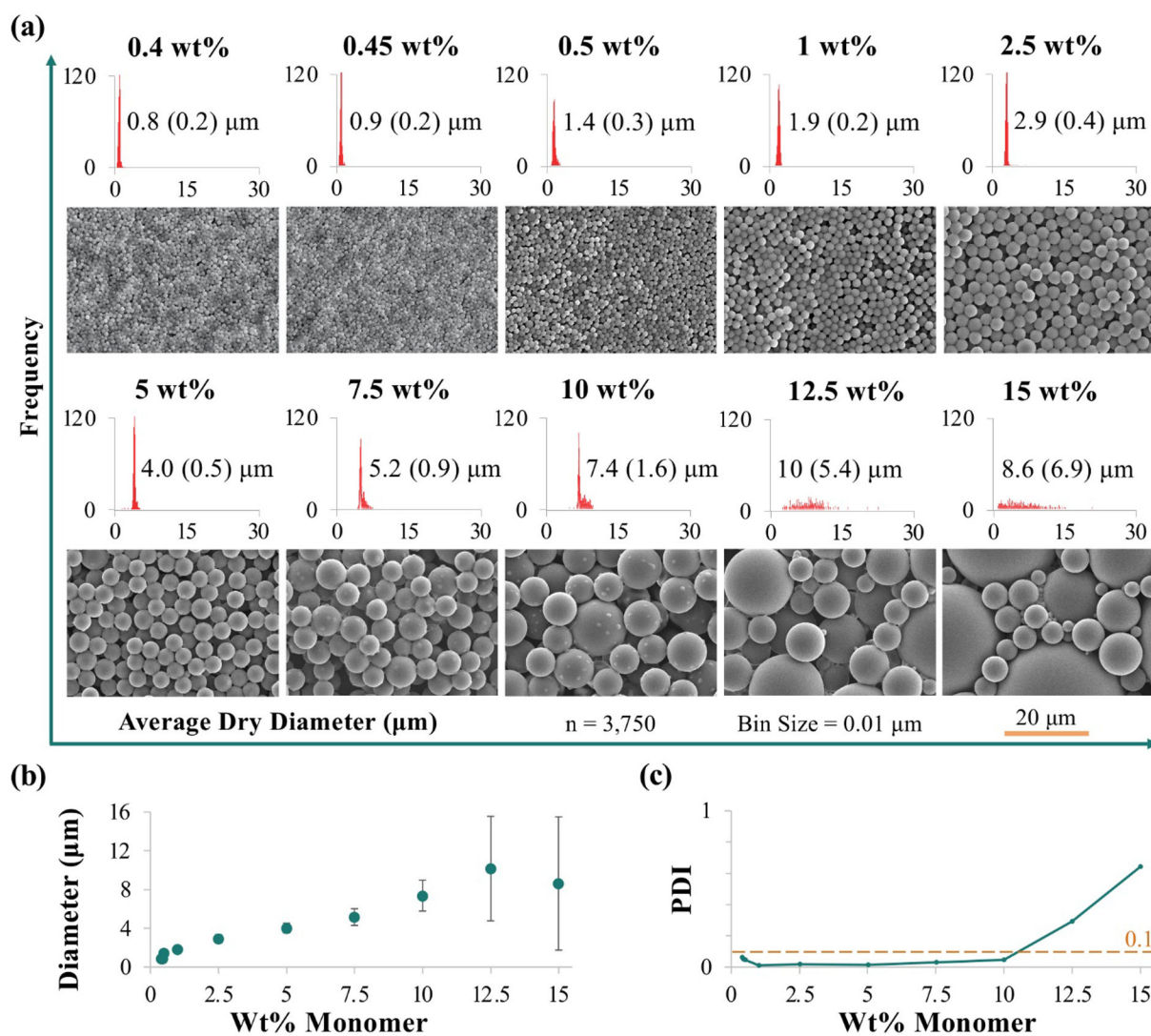
reacted with methyl maleimide to cap the free thiols; particles were at 4 mg/mL in buffers ranging from pH 3–9. Data presented as means with standard deviations as error bars.
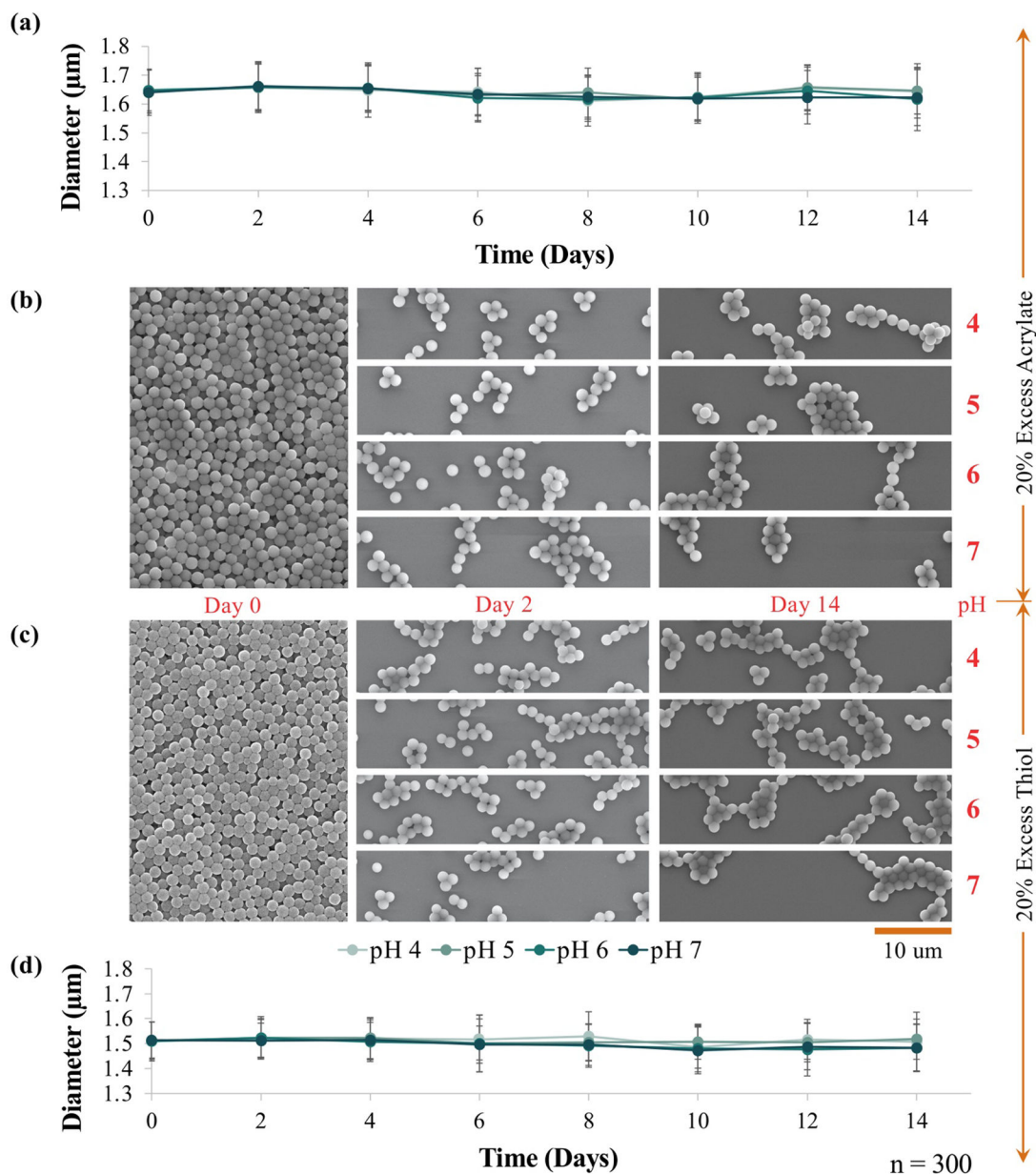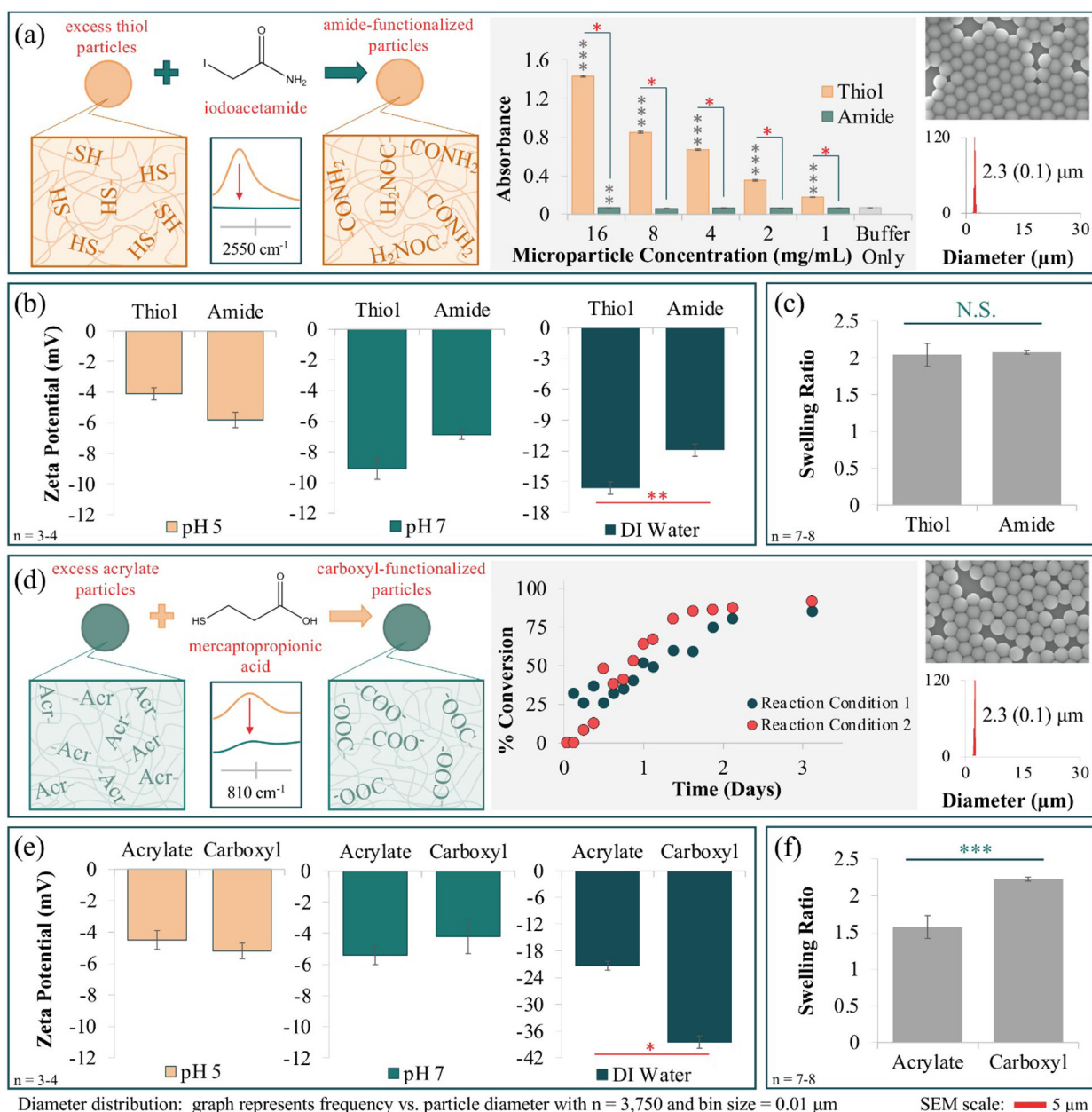
Figure 2.
(a) Representative SEM images are shown for 20% excess thiol microparticles synthesized at 0.4 – 15 weight percent (wt%) monomer along with the corresponding diameter distribution provided by histogram plots (n=3,750, bin size = 0.01 μm). (b) Particle diameter as a function of wt% monomer; data presented as means with standard deviations as error bars. (c) Polydispersity index (PDI) as a function of monomer wt%.
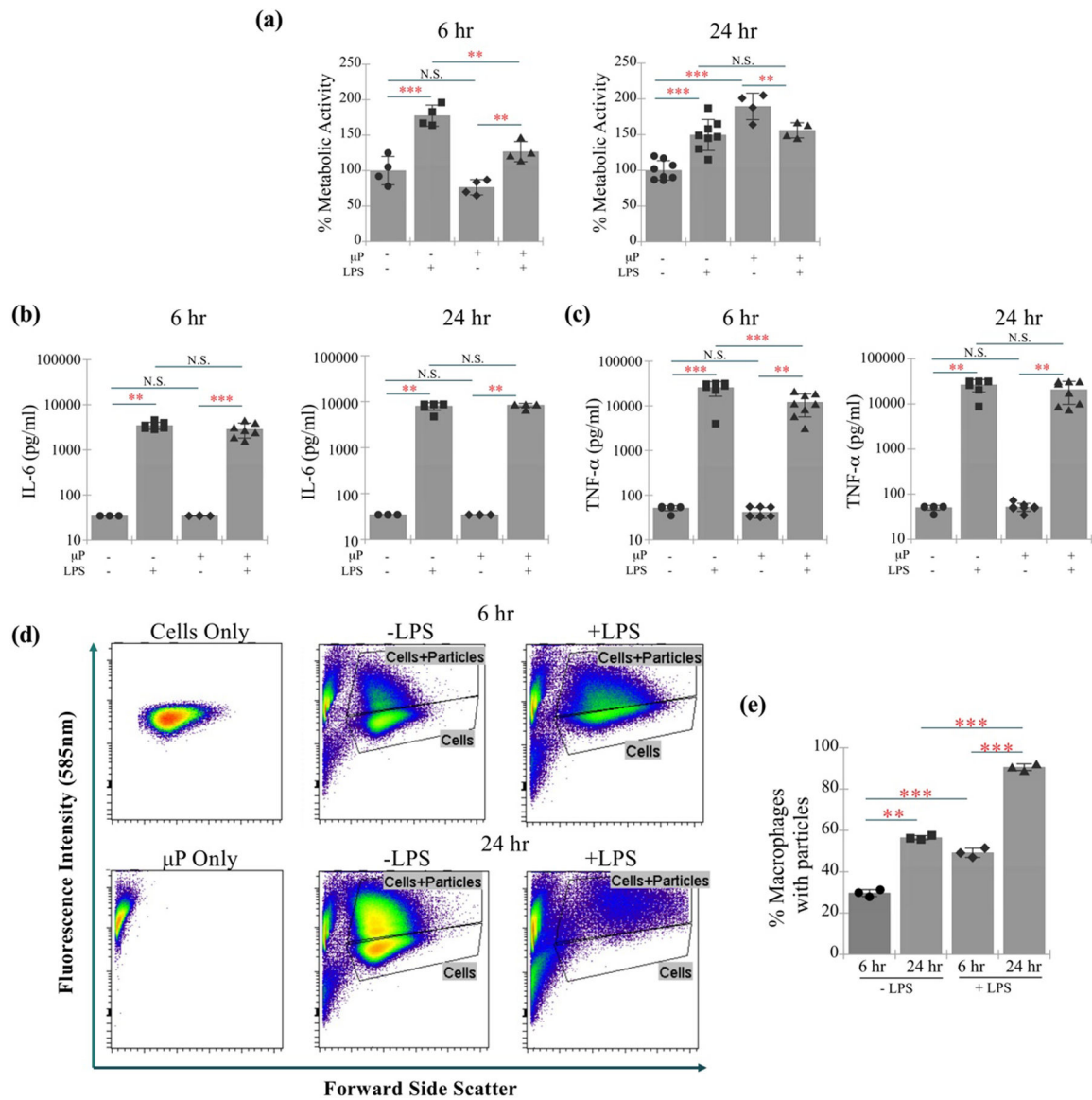
Figure 3.
Particles synthesized with 20% excess acrylate (a, b) and 20% excess thiols (c,d) at a concentration of 1 wt% monomer were soaked to buffers of pH 4, 5, 6, and 7, a range relevant to the phagosomal environment, over 14 days. Representative SEM images of the particles with subsequent diameter analysis (n=300) are shown. Data presented as means with standard deviations as error bars.
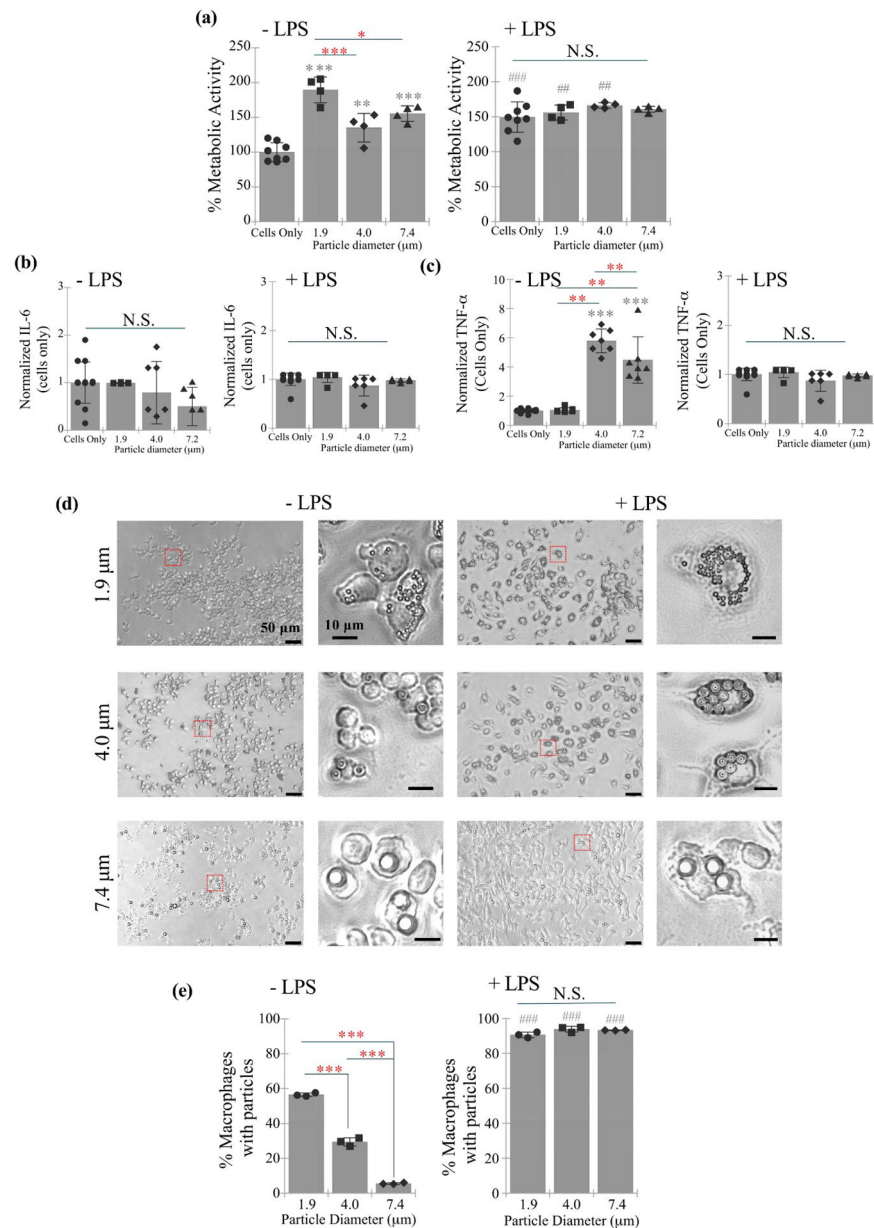
Figure 4.
(a) 33% excess thiol particles were reacted with iodoacetamide, yielding amide-functionalized particles as confirmed by disappearance of the sulfhydryl-associated FTIR peak at 2550 cm-1 relative to unreacted particles. Free thiols were quantified by absorbance from the Ellman's assay. Representative SEM image is shown along with histogram of diameters (n=300) and mean (standard deviation). (b) Zeta potentials of thiol and amide-functionalized particles were measured in buffers at pH 5 and 7 as well as filtered DI water at a particle concentration of 4 mg/mL. (c) Mass swelling ratios in filtered DI water are shown for the amide and excess thiol particles. (d) 33% excess acrylate particles were reacted with 3-mercaptopropionic acid to obtain carboxyl-terminated particles. Functionalization was confirmed by the reduction in the FTIR peak corresponding

to acrylates at 810 cm^{-1} and consumption of the acrylate functional groups was monitored using FTIR with ATR over 3 days for two reaction conditions with: 1% (reaction condition 1) and 2% (reaction condition 2) (g/v) 3-mercaptopropionic acid. SEM image is shown along with histogram of diameters (n=300) and mean (standard deviation) for reaction condition 1. (e) The zeta potentials of acrylate and carboxyl-functionalized particles at a concentration of 4 mg/mL were measured in buffers of pH 5 and 7 and in filtered DI water. (f) The mass swelling ratios in filtered DI water are shown for the carboxyl and excess acrylate particles. Data presented as means with standard deviations as error bars. Pairwise comparisons are shown for p<.05 by *, p<.01 by **, and p<.001 by ***. N.S. is not statistically significant.
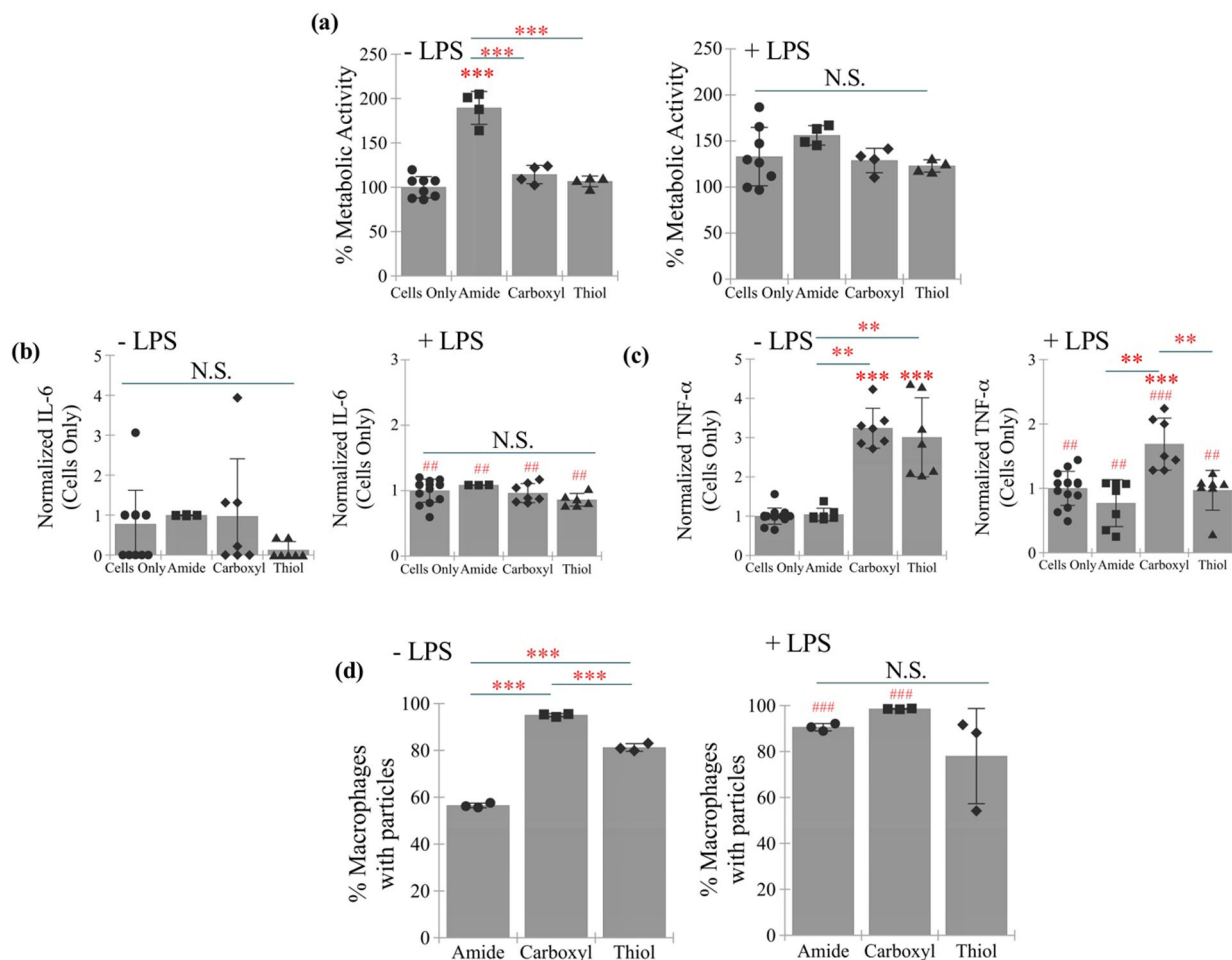
Figure 5.
Unstimulated and LPS-stimulated macrophages treated with or without 1.9 μm amide-terminated microparticles were assessed by (a) metabolic activity, (b) IL-6 production, and (c) TNF-α production at 6 and 24 hours. Metabolic activity (%) is reported relative to the control without microparticles and LPS at each time point. (d) Representative dot plots are shown for controls (cells only and microparticles only) and for each experimental group. (e) Dot plots were quantified for % macrophages with particles. Data presented as means with standard deviations as error bars. Pairwise comparisons are shown for p<.01 by ** and p< .001 by ***. N.S. is not statistically significant.
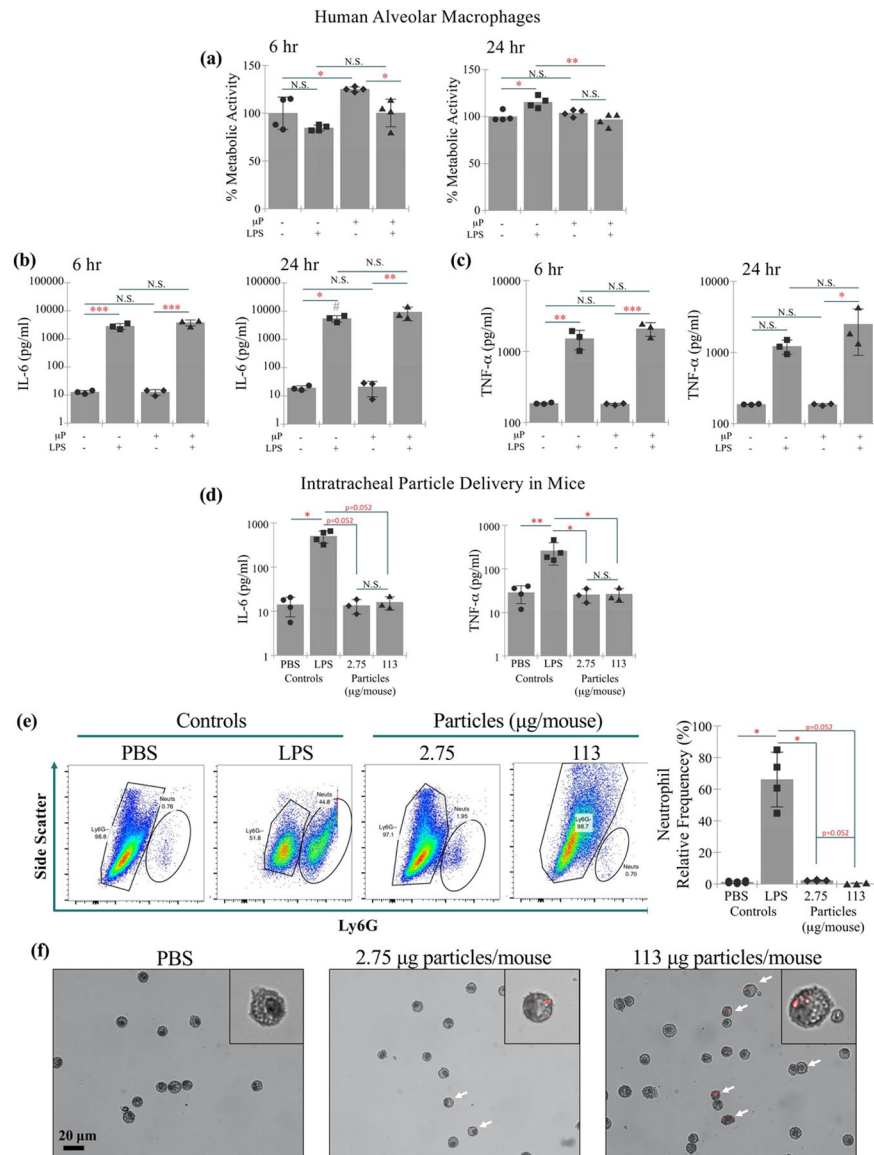
Figure 6.

Unstimulated and LPS-stimulated macrophages treated with or without amide-terminated microparticles of increasing diameter (1.9, 4.2, and 8.1 μm) with and without 1 μg/mL LPS were assessed by (a) metabolic activity, (b) normalized IL-6 production, and (c) normalized TNF-α production at 24 hours. Metabolic activity (%) is relative to the control without microparticles and LPS. IL-6 and TNF-α production were normalized to the cells only condition without LPS for the unstimulated macrophages and to the cells only with LPS condition for the stimulated macrophages. (d) Representative images of cells stained with May-Grünwald following 24 hours of microparticle treatment time with and without 1 μg/mL LPS. (e) % macrophages with particles determined by flow cytometry as a function of particle size with and without LPS. Data presented as means with standard deviations as error bars. Pairwise comparisons are shown: * above a column compares to cell only control,

* with bar denotes pairwise comparisons; # compares to no LPS condition for the same experimental group. Statistical significance is shown for $p<.05$ by one symbol, $p<.01$ by two symbols, and $p<.001$ by three symbols. N.S. is not statistically significant.

Figure 7.
Unstimulated and LPS-stimulated macrophages treated with amide, carboxyl, or thiol-terminated microparticles with and without 1 μg/mL LPS were assessed by (a) metabolic activity, (b) normalized IL-6 production, and (c) normalized TNF-α production at 24 hours. Metabolic activity (%) is relative to the control without microparticles and LPS. IL-6 and TNF-α production were normalized to the cells only condition without LPS for the unstimulated macrophages and to the cells only with LPS condition for the stimulated macrophages. (d) % macrophages with particles determined by flow cytometry as a function of particle chemistry with and without LPS. Data presented as means with standard deviations as error bars. Pairwise comparisons are shown: * above a column compares to cells only control, * with bar denotes pairwise comparisons; # compares to no LPS condition for the same experimental group. Statistical significance is shown for p<.05 by one symbol, p<.01 by two symbols, and p<.001 by three symbols N.S. is not statistically significant.

Figure 8.
Unstimulated and LPS-stimulated human alveolar macrophages treated with or without 1.9 μm amide-terminated microparticles were assessed by (a) metabolic activity, (b) IL-6 production, and (c) TNF-α production at 6 and 24 hours. Metabolic activity (%) is relative to the control without microparticles and LPS at each time point. Intratracheal delivery of 1.9 μm diameter amide-terminated microparticles to mice at concentrations of 2.75 μg and 113 μg particles/mouse *in vivo* was assessed for (d) IL-6 or TNF-α in BAL, (e) frequency of neutrophils in BAL shown by representative dot plots and quantification, and (f) representative images of cytospins. Control mice were treated with PBS or with LPS. Arrows identify alveolar macrophages with internalized microparticles, shown in red. Data presented as means with standard deviations as error bars. Pairwise comparisons are shown for p<0.05 by *, p<0.01 by ** and p<0.001 by ***. N.S. is not statistically significant.